# EVALUATION OF RISK OF PLASTIC SHRINKAGE CRACKING IN CONCRETE

Thalpe Guruge Pasindu Laknath Weerasinghe
158043 T

Degree of Master of Science

Department of Civil Engineering
University of Moratuwa
Sri Lanka

May 2017

# EVALUATION OF RISK OF PLASTIC SHRINKAGE CRACKING IN CONCRETE

Thalpe Guruge Pasindu Laknath Weerasinghe
158043T

Thesis submitted in partial fulfilment of the requirements for the degree Master of Science

Department of Civil Engineering
University of Moratuwa
Sri Lanka

May 2017

## DECLARATION

I declare that this is my own work and this thesis does not incorporate without acknowledgement any material previously submitted for a Degree or Diploma in any other University or institute of higher learning and to the best of my knowledge and belief it does not contain any material previously published or written by another person except where the acknowledgement is made in the text.

Also, I hereby grant to University of Moratuwa the non-exclusive right to reproduce and distribute our thesis, in whole or in part in print electronic or other medium. I retain the right to use this content in whole or part in future works (such as articles or books)

…… Date:

T.G.P.L. Weerasinghe

The above candidate has carried out research for the Masters Dissertation under my supervision.

…… Date:

Prof. S.M.A. Nanayakkara

## ABSTRACT

Plastic shrinkage cracking is a common phenomenon associated with concreting in hot and windy weather. Excess evaporation of bleed water causes loss of water from the concrete surface and plastic shrinkage occurs due to that at very early age i.e. within first 4-6 hours. Tensile strain will be developed as a result of this shrinkage and cracking will occur when it exceeds the tensile strain capacity of concrete

The measurement of tensile strain capacity of fresh concrete is important to predict the risk of plastic shrinkage cracking. Data on strain capacities at the very early age i.e during first few hours is hard to determine as concrete is still in fresh state. The report contains the procedure adopted to develop a simple test method to measure the local strain along a sample of fresh concrete. The influence of cement type, fine aggregate type and mortar phase for the strain capacity was studied. Results indicate that the addition of fly ash and manufactured sand has increased the tensile strain capacities.

In order to evaluate the risk of plastic shrinkage cracking it is necessary to develop a model to simulate strain development in fresh concrete due to plastic shrinkage. First, key factors affecting shrinkage, bleeding and evaporation, were modeled and the starting time of drying was identified. Subsequent loss of water was calculated and incorporated in a finite element model to simulate the tensile strain development. Calculated strains were very similar to the measured strains and therefore the model can be used to predict the development of early age tensile strain due to plastic shrinkage.

Tensile strain capacities determined from the test and the modeled strain development were compared to evaluate the risk of plastic shrinkage cracking in concrete with OPC and fly ash. Although there was an increase in strain capacity of concrete with fly ash blended cement, model predicted that the risk of cracking was higher in concrete with fly ash blended cement as there was a significant increase in strain developed as a result of drying. Further experimental studies are needed to prove the prediction and also to find the influence of other factors (PLC and admixtures) to plastic shrinkage cracking in concrete.



**Key words: plastic shrinkage cracking, tensile strain capacity, strain development model, finite element modeling**

## ACKNOWLEDGEMENT

I wish to thank University of Moratuwa and Department of Civil Engineering for providing me the opportunity to carry out this research. My sincere gratitude goes to Prof. S.M.A Nanayakkara for his guidance and support extended for the success of the research. I want to give special gratitude to all the staff members and lab assistants of department of civil engineering, University of Moratuwa for the help given by all means. And thanks to my colleagues for being so supportive in experiments. Finally I would like to thank Holcim (lanka) PLC for providing the necessary funding for the research.

# TABLE OF CONTENTS

# LIST OF FIGURES

# LIST OF TABLES

# 1 INTRODUCTION

## 1.1 Background

Concrete is the most widely used construction material in Sri Lanka. Concreting in hot and windy tropical climatic conditions is a challenging task as involves undesirable defects like plastic shrinkage cracking. Plastic shrinkage cracking is one of the most common defect reported in tropical countries. Plastic shrinkage occurs at the very early age when concrete is still fresh due to excessive evaporation of bleed water which results in drying of the concrete surface that could ultimately results in cracking. Over the past three decades, researches have been carried out to study the mechanism, the severity of it and the remedial measures to prevent such cracks. However still there is no universal method to assess the risk of plastic shrinkage cracking in concrete.

Earlier, the understanding was that plastic shrinkage cracking was purely because of excessive evaporation. Relying on the critical evaporation rate of water from free concrete surface recommended by ACI and precautions were taken when evaporation rate is greater than the critical limit to prevent plastic shrinkage cracking. However, cracks have been observed even below the prescribed evaporation rate which implies that plastic shrinkage cracking does not purely depend on evaporation.

Recent studies explain that plastic shrinkage is governed by both bleeding and evaporation. Since bleeding depends on the mix proportion, plastic shrinkage depends on both mix proportion and external environmental factors. Therefore to predict the occurrence of such cracks the amount of bleeding, evaporation rate and the shrinkage strain should be evaluated for different mix proportions under different environmental conditions.

As plastic shrinkage cracking is mainly due to tensile strain development as a result of volume change, tensile strain capacity of concrete and the tensile strain development due to shrinkage govern the probability of such occurrence. However, measuring strain capacity of fresh concrete is a challenging task as the concrete is still in semi-liquid phase.

Development of a new test method to measure the tensile strain capacity of fresh concrete and development of an analytical and finite element model to predict the tensile strain development in fresh concrete is presented. Based on the two parameters, evaluation of the risk of plastic shrinkage cracking is discussed in the thesis.

## 1.2 Objectives

The primary objective of this research is to evaluate the risk of plastic shrinkage cracking in concrete, based on tensile strain capacity of fresh concrete and early age strain development. In order to accomplish this objective following tasks were considered.

- Development of a test method to measure the tensile strain capacity of fresh concrete and study the influence of mix parameters on the tensile strain capacity
- Development of a finite element model to predict the tensile strain development of fresh concrete

## 1.3 Methodology

The following steps were carried out in order to achieve the above objectives.

- A comprehensive literature review was carried out in order to identify the plastic shrinkage mechanism and current test methods used to measure tensile strain capacity of fresh concrete.
- A new test method was developed to measure tensile strain capacity of fresh concrete while overcoming the drawbacks identified from the previous test methods.
- The influence of cement type, mortar phase and type of fine aggregates on the strain capacity was studied using the new test method.
- An analytical model was developed to predict the bleeding behavior of concrete.
- A finite element model was developed to predict the tensile strain development of fresh concrete.

- The risk of plastic shrinkage cracking was evaluated using the above test method and strain development model.

## 1.4 Arrangement of Thesis

- Chapter 2 of the thesis presents the findings of the literature review.
- Chapter 3 provides the details of the test method used to determine tensile strain capacity and the results obtained.
- Chapter 4 highlights the modeling of shrinkage development in fresh concrete and the verification of the proposed model
- Chapter 5 presents the evaluation of risk of plastic shrinkage cracking for concrete produced with OPC and fly ash blended cement.
- Chapter 6 presents the conclusions

# 2 LITERATURE REVIEW

## 2.1 General

Concrete is the most widely used construction material in Sri Lanka as well as in the whole world. Many researches have been done to identify and if possible prevent or minimize early age cracking in concrete as this will significantly affects the durability of concrete in the long term. Among many forms of cracks in concrete, plastic shrinkage cracking is very common in Sri Lanka and often neglected without knowing the fact that other forms of shrinkage such as drying shrinkage and thermal contraction would widen these cracks and cause detrimental effects later.

The literature review was carried out in the aim of understanding the mechanism of plastic shrinkage and to identify a method to evaluate the risk of plastic shrinkage cracking. The findings presented are twofold. The first aspect is on developing a test method to measure the tensile strain capacity of fresh concrete and the second aspect is on the tensile strain development of fresh concrete. The ultimate aim is to develop a method to predict the risk of cracking using the tensile strain capacity and the tensile strain developed in fresh concrete.

## 2.2 Determination of tensile strain capacity of fresh concrete

Plastic shrinkage cracking is a common phenomenon associated with concreting in hot and windy climatic conditions. These cracks, which occur mostly on horizontal surfaces, usually develop as the water sheen disappears from the surface of concrete. Ambient temperature, relative humidity, wind velocity, concrete temperature and bleeding characteristics of concrete are some of the factors which influence plastic shrinkage cracking of concrete (Almusallam et al., 1997).

Measuring physical properties of fresh concrete is important to understand the behaviour of the concrete at early age. Plastic shrinkage occurs at the very early stage due to evaporation of water from the concrete surface. When concrete is restrained

against plastic shrinkage, tensile strain is developed and when it exceeds the tensile strain capacity, cracks occur. This phenomenon is called as plastic shrinkage cracking

Shrinkage of concrete cannot be avoided. It will occur due to at least the volume reduction resulting from the hydration of cement and water, which consumes less space than the initial products. Shrinkage of concrete takes place in two distinct *stages*: early and later ages (Holt, 2004). The early age is commonly defined as the first day, while the concrete is setting and starting to harden. Later ages, or long-term, refers to the concrete at an age of 24 h and beyond. At early ages, the risk of cracking is generally high because of the significant increase of shrinkage and the relatively low strength of concrete (Hammer et al., 2007).

The above theory is validated by the tests carried out by several researchers (Kasai, 1968 and Weigler & Karl, 1974 and Byfors, 1980). Although it is not clear how they measured these values, they indicate that tensile strain capacity reaches the lowest value before 10 hours and then it increases again (see Figure 2.1).

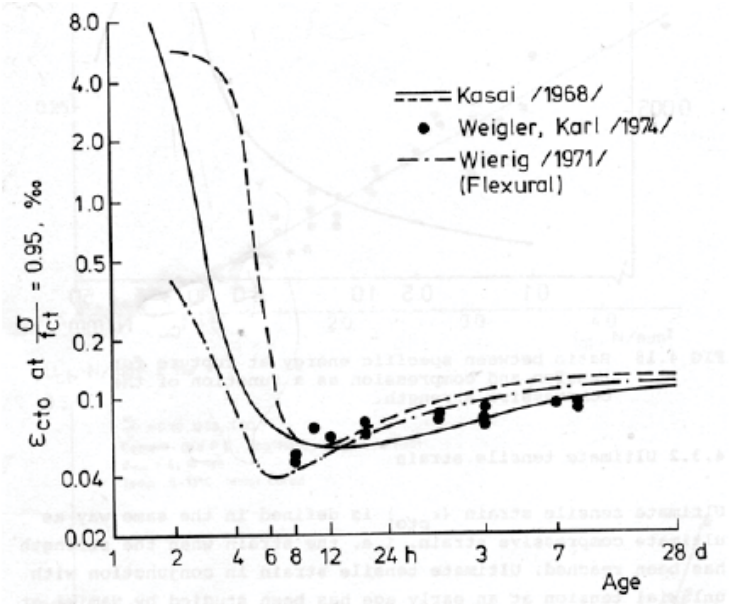


**Figure 2.1 Tensile strain at 95% of ultimate tensile stress vs age (Byfros, 1980)**

Hammer has identified that strain capacity also varies with the strain application rate (Hammer, 2007). Results of the experimental investigation done by Roziere also confirm the above explanation (Roziere et al., 2015) (see Figure 2.2). It shows that at a higher strain rate, the variation of the tensile strain capacity was more similar to what previous experiments have measured as shown in Figure 2.1.

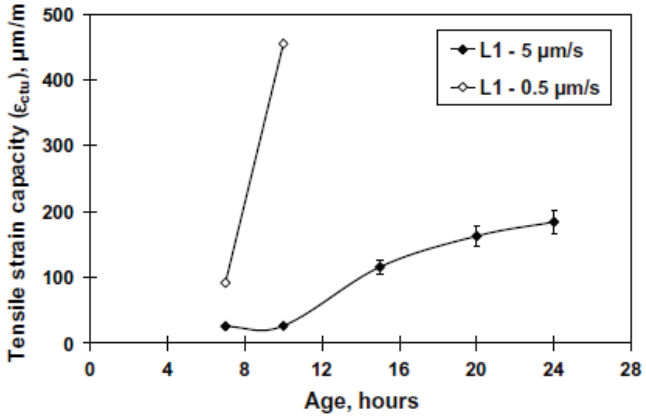


**Figure 2.2 Variation of tensile strain capacity with strain rate**

### 2.2.1 Strain Measuring Techniques

Greim has summarized the techniques to measure early shrinkage of mortars (Greim, 2011). According to him, material at early ages have three distinguish ranges of material strengths which are fluid, starting of setting and hardened material which needs different measurement techniques. Two major types of sensors were identified as contacting sensors and contactless sensors.

Kasai has used strain gauges which was a contacting sensor. A strain gage is a thin foil, sized several millimeters, with an electrical resistor network printed on. If a thin wire is elongated the diameter of the wire will decrease and the resistance will increase. So the resistance is an indication of the deformation.

Hannat has used LVDTs (Linear Variable Differential Transformers) which was also a contacting sensor (Hannat et al., 1999). The LVDT has a movable ferromagnetic core. Depending on the position of the core, the voltage inducted from the primary to the secondary coil is changed.

Contactless sensors available are ultrasound, inductive sensors, laser TOF (Time of Flight), laser triangulation and capacitive type sensors. However, these sensors are very expensive ranging from £1,000 to £10,000 (Greim, 2011).

Emphasis was made on using Digital Image Correlation (DIC) to determine concrete strain (Huang et al., 2010). It is a handy, reliable and cost effective method and can be automated to measure real-time strain variation. As it is a contactless method, it's more suitable for fresh concrete strain measurement. Roziere used the difference between displacements of regions from two images to assess the displacement of the fresh concrete specimen (Roziere et al., 2015).

### 2.2.2 Influence of various factors on Tensile Strain Capacity

Kasai has studied the influence of different cement types and loading rate on the tensile strain at 95% of ultimate tensile stress (Kasai et al., 1972). Results are shown in Figure 2.3.

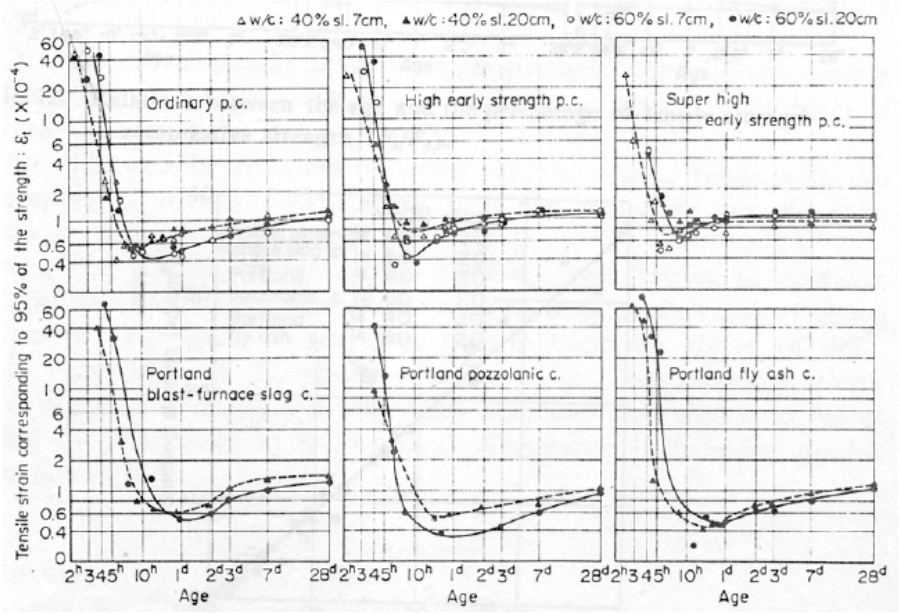


**Figure 2.3 Tensile strain at 95% of ultimate tensile stress vs age of various concretes (Kasai et al, 1972)**

Hammer has studied about high strength concrete and tensile strain capacity as an indication to cracking at early age (Hammer, 2007). He changed the parameters such as water/cement ration, cement type, the plasticizer composition and time of drying. Point where negative pore water pressure reaches its minimum value was taken as the crack initiation time (t). Tensile strain capacity was defined as strain at which first crack appears. Then ;

Strain capacity ($\varepsilon_t$) = Strain rate ($\varepsilon$/unit time) * time at which first crack occurs (t)

Roziere studied on the influence of aggregate type on tensile strain capacity. According to his findings strain capacity was not significantly affected by the aggregate type (Roziere et al., 2015) (see figure 2.4).

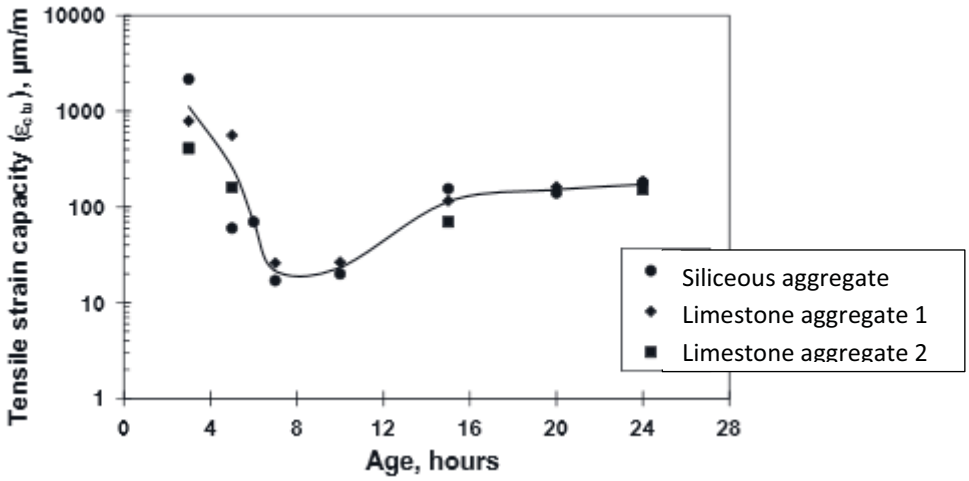


**Figure 2.4 Tensile strain capacity for different aggregate types ( E. Roziere et al, 2015)**

## 2.3 Tensile strain development in fresh concrete

When freshly placed concrete is exposed to the environment, a portion of water is removed from concrete due to evaporation. In order to account for this volume loss the concrete shrinks and a tensile strain is being developed as a result of this shrinkage. It can be found from the literature that bleeding (which is the process of forming a thin layer of water on top of freshly placed concrete) and evaporation (which is the process of removal of water due environmental factors such as temperature, wind speed and

relative humidity) are the key factors which develops tensile strain in fresh concrete (Radocea, 1994 and Combrinck & Boshoff, 2013).

### 2.3.1 Bleeding

The accumulation of water over a period of time at the surface of freshly mixed cement paste, mortar, or concrete is known as 'bleeding' (Josserand at al., 2006). Gravitation is the predominant force which causes the solid particles to settle and induces an upward displacement of water to the top surface. Bleeding process continues until the cement paste get consolidated or set.

Numerous researches have been conducted to measure the bleeding behavior of fresh concrete (Almusallam et al., 1997 and Topcu et al., 2004). However, there are few published papers on modeling the bleeding behavior without experimentally measuring it. Among them, Tan et al. has proposed a reasonably accurate numerical model to predict bleeding (Tan et al., 1987) and it has been used and improved by other researches (Kwak & Ha, 2006 and Morris & Dux, 2010).

The analytical model was based on the self-weight consolidation of cement paste. The solid particles are closely packed and there are inter-particle forces acting between them and therefore a consolidation model is used to explain the bleeding. Detailed derivation of the consolidation model can be found in literature (Tan et al., 1987). The governing equation for bleeding is as follows (eq. 2.1).

$$\frac{\beta K_0}{\gamma_w}\frac{\partial^2 e(z,t)}{\partial z^2} = \frac{\partial e(z,t)}{\partial t} \qquad \text{……..……..(2.1)}$$

In the above equation β and $K_0$ are constants determined from the mix proportion of the concrete, whereas $\gamma_w$ is the unit weight of water. Symbol *e* is the water to solid ratios by volume at time t and z denotes the height of solids.

The governing equation was applied for a certain boundary condition as shown in Figure 2.5 and the amount of bleeding was calculated as follows (Tan et al., 1987).

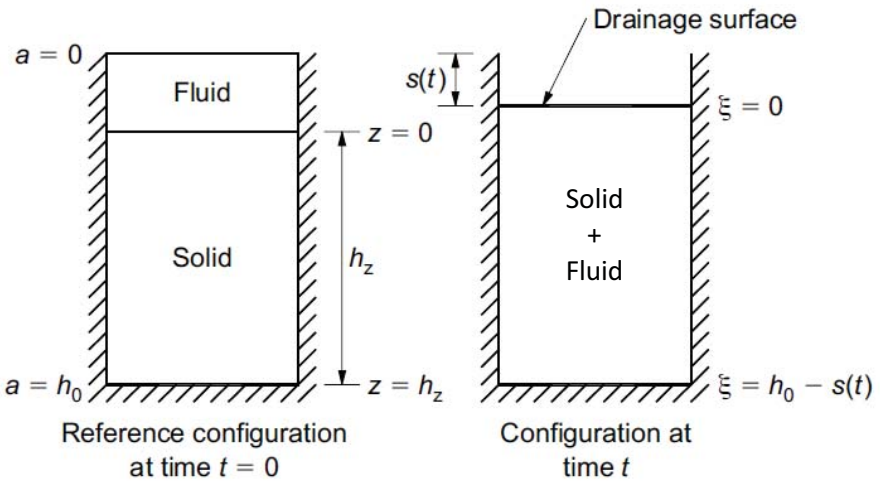


**Figure 2.5 Bleeding model by Tan et al**

(a) At time t=0, e(z,0) = $e_0$ (Initial water to solid ratio was taken as $e_0$ )

(b) At the top surface z=0, e(0,t) = $e_0$ (At any given time t, water to solid ratio at the top surface was taken as $e_0$ because there is a thin layer of water formed on the top surface )

(c) At the bottom impervious surface z=$h_z$, de/dz=($\gamma_w$–$\gamma_s$ )/ β where $\gamma_s$ unit weight of cement.

The amount of bleeding is equivalent to the surface settlement s(t) and can be calculated by the following equation (eq. 2.2) where $h_0$ is the initial height of the concrete sample.

$$s(t) = h_0 - \int_0^{h_z} [1 + e(z,t)]dz \qquad \text{……..….(2.2)}$$

Determination of $K_0$ and β (see eq. 2.1) factors for a given mix was further simplified by Kwak et al. and he has proposed following regression formulas (eq. 2.3 and 2.4) (Kwak & Ha, 2006).

$$K_0 = K_{0,ref}.\lambda_{K_o,w/c}.\lambda_{K_o,W}.\lambda_{K_o,s/a}.\lambda_{K_o,H} \qquad \text{……..….(2.3)}$$

$$\beta = \beta_{ref}.\lambda_{\beta,w/c}.\lambda_{\beta,W}.\lambda_{\beta,s/a}.\lambda_{\beta,H} \qquad \text{……..….(2.4)}$$

Regression coefficients corresponds to water/cement ratio (w/c), unit water content (W), sand to aggregate ratio (s/a) and the depth of the concrete (H) respectively. These coefficients have been proposed after comparing modeled bleeding behavior with various other independent experiments done. A reference mix have been taken to determine $K_{0,ref}$ and $\beta_{ref}$ values. The reference mix consisted of a concrete mixture having w/c = 50%, W =175 kg/m$^3$, s/a = 46 % and H = 25 cm respectively. Following Figures (2.6 to 2.9) shows the regression coefficients determined (Kwak & Ha, 2006).

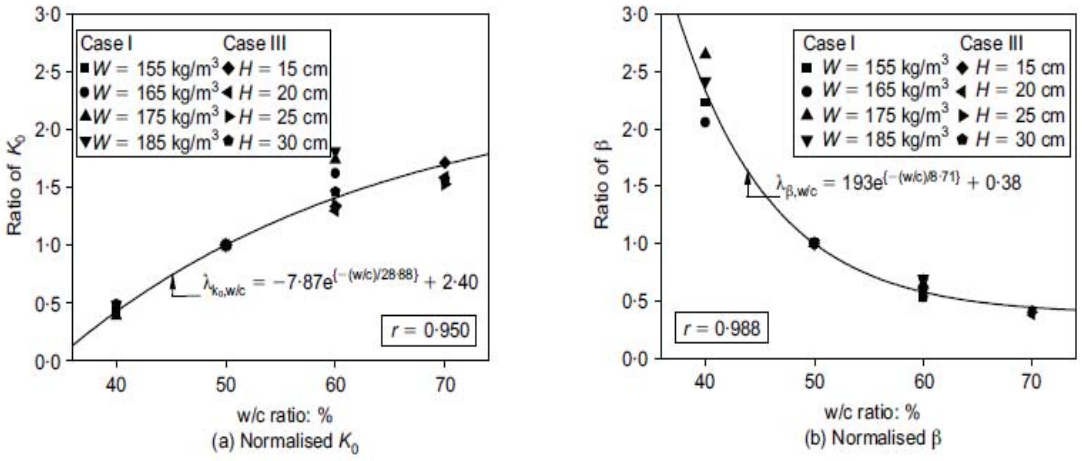


**Figure 2.6 Regression coefficients for w/c ratio**

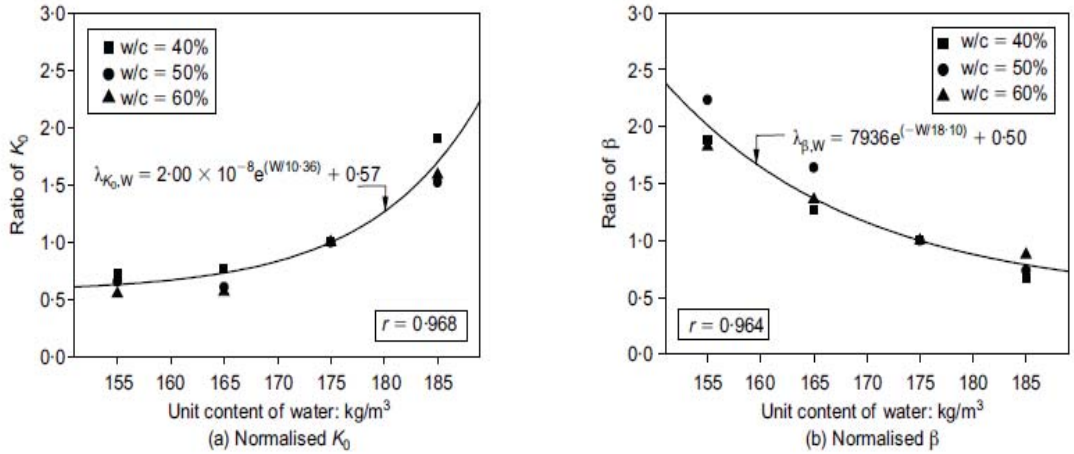


**Figure 2.7 Regression coefficients for unit water content (W)**

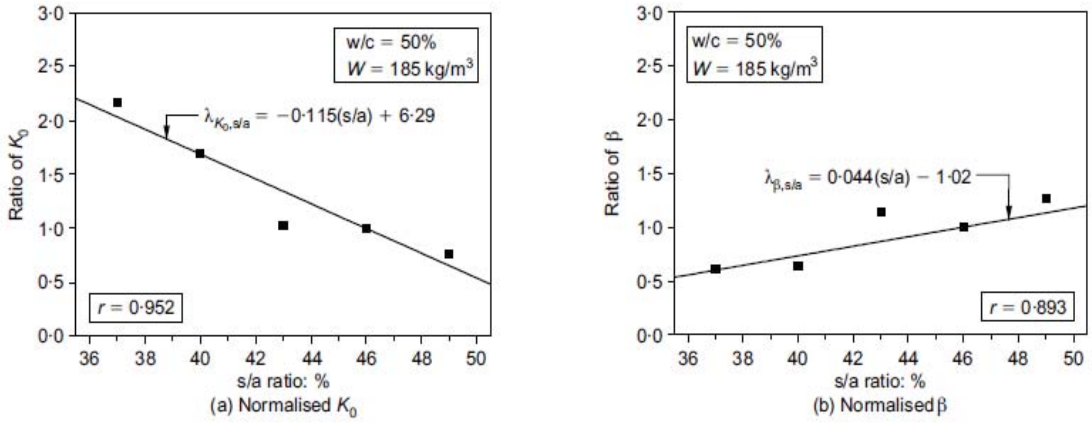


**Figure 2.8 Regression coefficients for sand/aggregate ratio (s/a)**

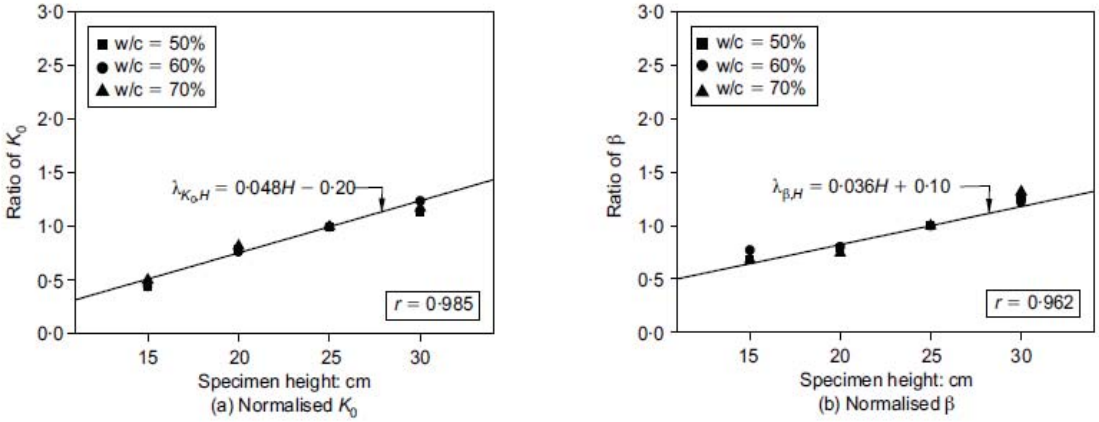


**Figure 2.9 Regression coefficients for specimen height (H)**

### 2.3.2 Evaporation

Evaporation is the process by which a liquid is converted into a vapor or gas. Environmental factors such as wind, air temperature, humidity and water surface temperature play a key role in evaporation (Uno, 1998). Plastic shrinkage cracking is common in countries with tropical weather conditions. Main reason is the hot and windy climatic conditions prevailing in those countries which accelerate the rate of evaporation. According to report by ACI Committee 305(ACI committee, 1999), the principal cause of plastic shrinkage cracking of Portland cement concrete is the excessive and rapid rate of evaporation of water from the surface of concrete and the inability or lack of bleed water to replace the evaporating water (Almusallam et al., 1997). ACI report proposes a value of 1.0 kg/m$^2$/h as the critical rate of evaporation

which if exceeded the risk of plastic cracking is extremely high. But it was noted that plastic shrinkage cracking could occur at evaporation rates as low as 0.2 kg/m$^2$/h to 0.7 kg/m$^2$/h (Almusallam et al., 1997). Therefore it is important to consider combined effects of both evaporation and bleeding to tensile strain development which results in plastic shrinkage cracking.

Evaporation from a concrete surface can be experimentally determined by weighing the sample continuously and the corresponding weight loss can be taken as the weight of evaporated water (Slowik et al., 2008). For the modeling of evaporation, the most widely used technique is the ACI monograph (ACI committee, 1999) (Figure 2.10).

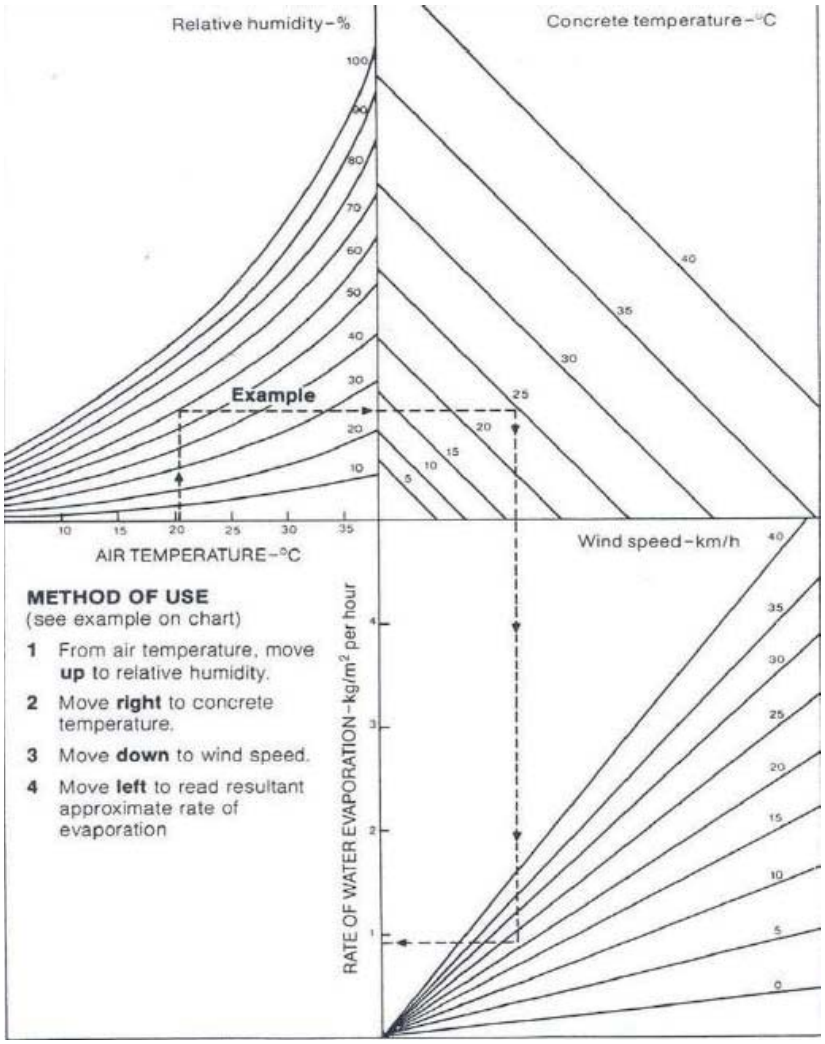


**Figure 2.10 ACI nomograph to predict the evaporation rate**

For a given atmospheric temperature, relative humidity, concrete surface temperature and wind velocity, evaporation rate can be determined using the above monograph. Or else following equation (eq. 2.5) can also be used to accurately predict the rate of evaporation (Uno, 1998)

$$ER = 5\left[(T_C + 18)^{2.5} - \frac{RH}{100}(T_A + 18)^{2.5}\right](V + 4) \times 10^{-6} \quad \text{.....(2.5)}$$

ER – Evaporation rate ( $kg/m^2/hr$ )

$T_c$ – Concrete temperature ($^0C$)

RH – Relative humidity as %

$T_A$ – Ambient temperature ($^0C$)

V- Wind velocity (km/h)

### 2.3.3 Measuring Strain Development

A thin layer of water is formed at the top surface of concrete because of bleeding. As long as this water layer is present, there will be no loss of volume from the concrete, hence plastic shrinkage would not occur. If the surrounding environmental conditions such as temperature, wind and humidity promote evaporation, gradually the bleed water will get evaporated and ultimately if the evaporation rate is higher than bleeding rate, the thin water layer will completely disappear. If evaporation continues, water within the concrete will start to get evaporated. This instance can be regarded as the point of drying. Shrinkage will occur after this drying point.

A tensile strain would develop as a result of this shrinkage and it was first measured by Wittmann in 1976 and Figure 2.11 shows what he has observed (Wittmann, 1976). After that, several other researchers also did experimental investigation on the strain development of fresh concrete and the pattern they observed is similar to one another (Slowik et al., 2008 and Hammer, 2007). Tensile strain has started to develop after the point of drying and has gradually increased for a certain period of time and then

reached a limiting value (see figure 2.12 and 2.13). The reason found from the literature is illustrated in Figure 2.14.

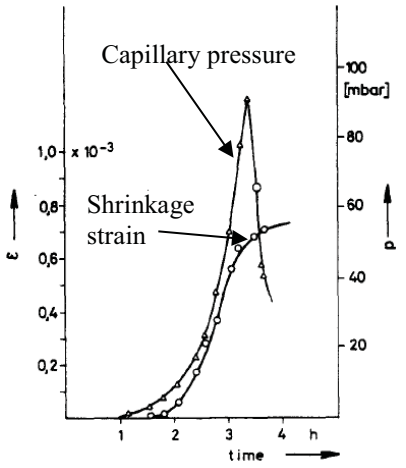


**Figure 2.121 Capillary pressure development (Wittmann, 1976)**

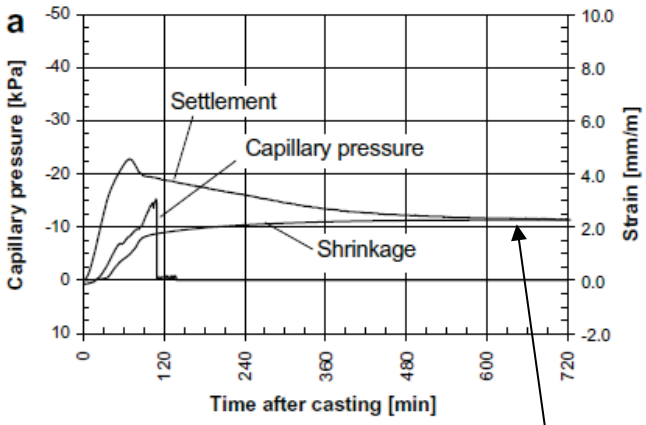


**Figure 2.112 Capillary pressure development and shrinkage strain (Slowik et al., 2008)**

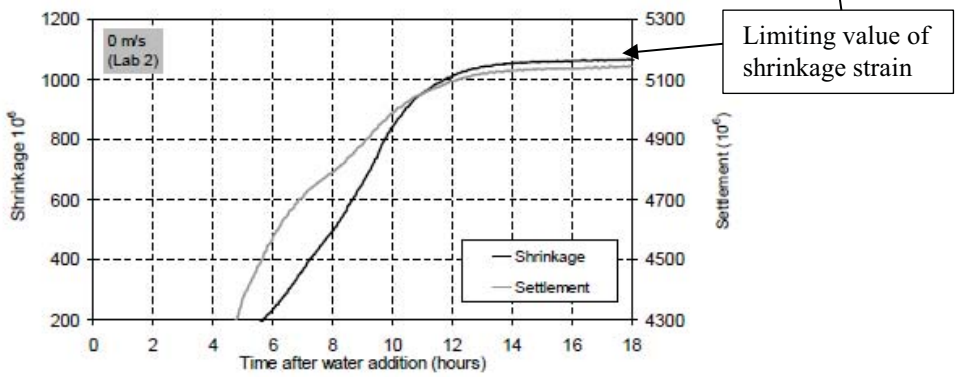


**Figure 2.13 Shrinkage strain development (Hammer, 2009)**

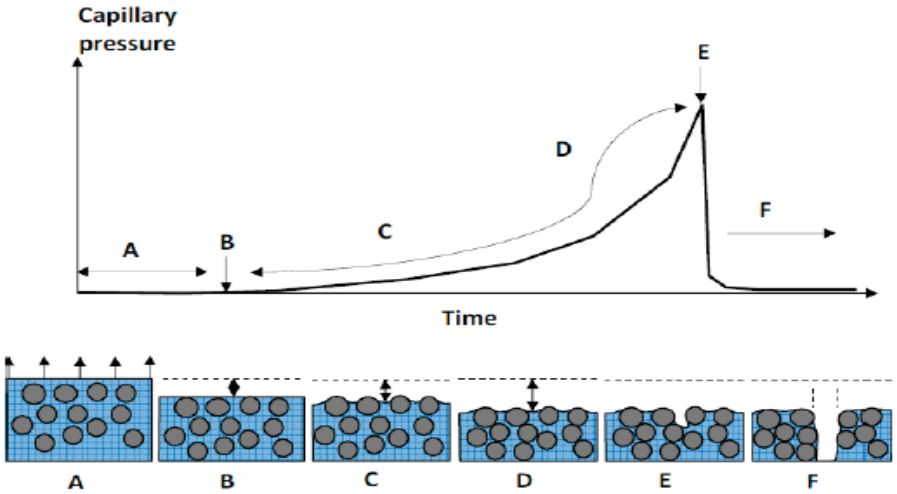


**Figure 2.14 Capillary pressure development mechanism (Combrinck, 2011)**

**A -** During this stage a thin film of water is present on the concrete surface. The rate at which bleed water is transported to the surface is initially higher than the rate at which it evaporates. The result is an accumulation of bleed water on the surface.

**B -** At this point there is no longer a thin film of bleed water on the concrete surface. The amount of bleed water that has been transported to the surface is equal to the water that has evaporated from the surface. This point indicates the start of capillary pressure build-up.

**C -** As the evaporation rate exceeds the bleed rate, menisci gradually form between solid particles and result in an increasing contraction effect and a subsequent capillary pressure build-up.

**D -** Capillary pressure has a vertical and horizontal component. At this stage the vertical component of capillary pressure forces the solid particles downwards. This results in the displacement of free water upwards, which has a decreasing effect on the capillary pressure (Powers, 1968). Despite this the rate of capillary pressure build-up is still on the rise (Slowik, et al., 2008).

**E -** Once the capillary pressure, known as the air entry or breakthrough value, is reached, the radii of the water menisci on the surface become too small to bridge the pore spaces between solid particles on the concrete surface and air entry occurs. The localized zones of air entry can be seen as weak points from a mechanical point of view (Slowik, et al., 2008).

**F -** Between the weak zones of air entry the capillary pressure continues to build-up. Localization of strain occurs in these weak zones as the concrete continues to shrink horizontally. When the shrinkage is restrained, tensile stresses build up until they inevitably exceed the tensile strength of the concrete over these weak zones, causing cracking.

After the point of air entry (E) further shrinkage does not occur and it reaches a limiting value. Therefore it is needed to identify the starting point of strain development and the time it reaches the limiting value in order to model the tensile strain development in fresh concrete. By comparing the developed strain and the strain capacity of fresh

concrete the risk of plastic shrinkage cracking can be predicted without doing any experiments.

## 2.4 Risk of plastic shrinkage cracking

Risk of plastic shrinkage cracking is directly associated with the rate of evaporation which is an external factor governed by the environmental conditions and the rate of bleeding which is an internal factor that depends on the concrete mix proportion, water content, amount of fines (cement, fly ash, fine sand, etc.) and the depth of concrete placed (Kwak et al., 2006). Therefore mix composition significantly affects the risk of plastic shrinkage cracking.

According to experimental investigations lean-stiff mixes (relatively low bleeding) has cracked earlier than rich plastic (relatively high bleeding) mixes. However the crack intensity is less in lean-stiff mixes than rich plastic mixes. (Almusallam et al., 1998). Furthermore, plastic shrinkage cracking is increased in high strength concrete (or high cement contents or low w/c ratios) (Dias, 2003). It suggests that the risk of plastic shrinkage cracking is increased when the bleeding rate is low (Uno, 1998).

ACI proposes a value of 0.5 $kg/m^2/h$ for the evaporation rate and beyond this value precautions should be taken to prevent plastic shrinkage cracking. If the evaporation rate is more than 1.0 $kg/m^2/h$ the guideline says plastic shrinkage cracks are most likely to occur. Higher the rate of evaporation, the risk of plastic shrinkage cracking is high as it quickly dries up the surface and remove moisture from concrete which ultimately results in development of plastic shrinkage.

Boshoff has proposed the following equation to estimate the plastic shrinkage cracking risk (PSC Risk) (Boshoff, 2012).

PSC Risk = (Plastic Period x Evaporation Rate) – Bleeding Volume – Fibre Risk reduction

It was based on the experimental results which indicate that higher evaporation rates and lower bleeding rates increase the chance of plastic shrinkage cracking. Furthermore, it was also found that adding micro synthetic fibres substantially increased interfacial shear bond stress between the cement paste and the fibres near the

initial setting time of concrete when plastic shrinkage cracking is expected to start (Combrinck & Boshoff, 2013). Therefore adding fibres has resulted in reducing the plastic shrinkage cracking.

## 2.5 Summary

Plastic shrinkage cracking is often occurred when concreting in hot and windy climatic conditions. It occurs in the very early age (fresh) of concrete and the main factors that govern plastic shrinkage are bleeding and evaporation. Bleeding depends on the mix parameters and evaporation depends on the external environmental factors. When the evaporation rate is higher than the bleeding rate, it results in removal of moisture from the top surface of concrete and as a result of this volume loss, a tensile strain is being developed. When it exceeds the tensile strain capacity of fresh concrete, cracking starts. Over the years, researchers have developed numerous test methods to determine the tensile strain capacity of fresh concrete but there are drawbacks. Therefore, a simple yet accurate test method is needed. Extensive studies were done to identify the mechanism of strain development in fresh concrete and few researchers have measured the strain. However, no attempt was done to model the strain development. By modeling the early age strain development and comparing it with the measured tensile strain capacity, the risk of plastic shrinkage cracking can be predicted.

# 3 EXPERIMENTAL PROGRAM AND ANALYSIS

## 3.1 General

Based on the literature survey, following procedure was adopted to develop a test method to measure the tensile strain capacity of fresh concrete. Figure 3.1 shows the methodology flow chart.

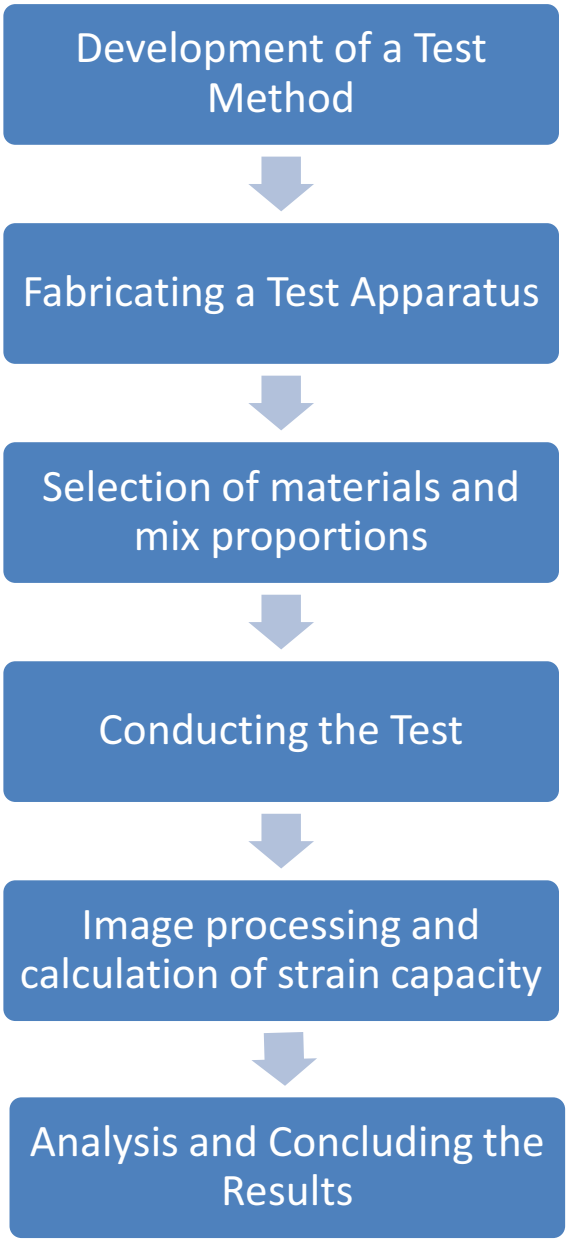


**Figure 3.1 Methodology Flow Chart**

Previous experiments carried out were concerned about measuring both tensile strain capacity and tensile stress in fresh concrete. Therefore, a novel test method has to be developed which is simple and cost effective. The results should be accurate and should be obtained easily. Development of such a test method, test procedure and analysis of results are further discussed below.

## 3.2 Development of a Test Method

Based on the literature survey, following key features were identified that should be addressed when developing a test method to test fresh concrete.

- Sample should be placed on a mould or casing to support it, as fresh concrete is in semi-liquid state and it can flow.
- Strain should be applied to the mould and the mould will transfer it to the concrete.
- Contactless method should be adapted to measure strain.
- Measuring strain distribution along the sample give more accurate results than average strain throughout the sample.
- Test should be repeatable.

Taking the above features into account, the following test method was developed.

- Concrete was placed on a rubber mould.
- Rubber mould was fixed at one end and pulled from the other end. Concrete sample inside will move along with it thus the strain applied would be transferred to the sample.
- Markers were placed on the sample which will act as reference points to measure strain.
- A camera placed above the sample was used to capture images continuously from the start until to the point of appearance of the first crack.

- Images were analyzed and pixel count (modified by a scale factor) between two markers at the beginning and at the crack initiation point was used to calculate strain at failure.

### 3.3 Fabricating a Test Apparatus

Literature survey pointed out following problems to overcome when fabricating a test equipment.

- Gripping the sample firmly so that a tensile load can be applied
- Placing the sample in a test machine
- Elimination of friction between the sample and its support plates
- Measurement of strain on a wet, plastic material
- Damage to the developing microstructure which might influence the measured properties, i.e. the measuring method must not disturb the sample under test.

Figure 3.2 shows the apparatus fabricated.

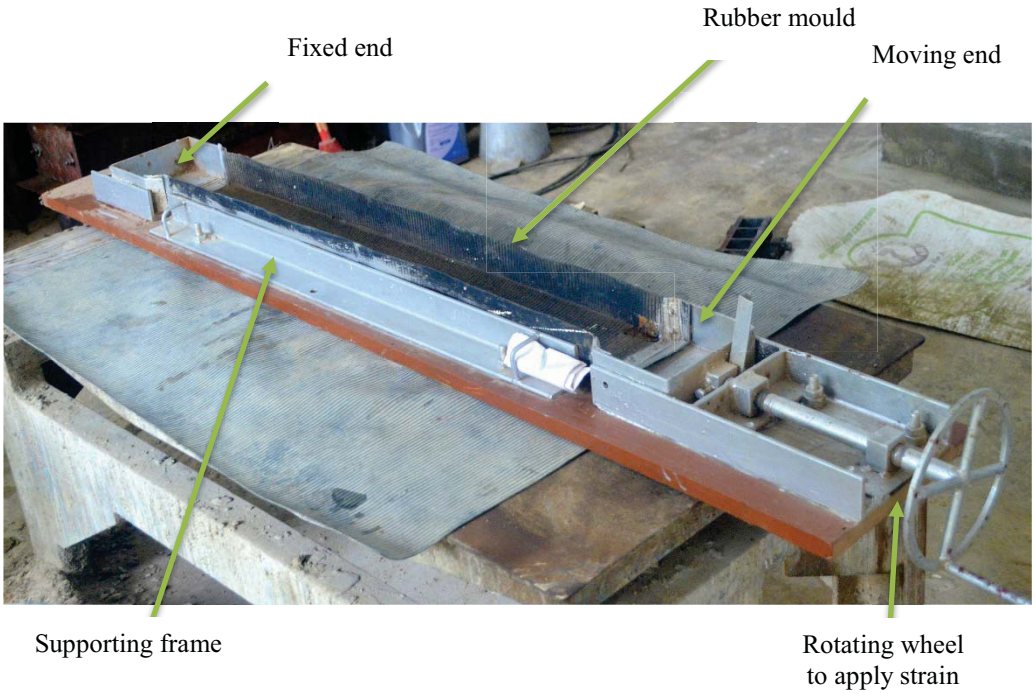


**Figure 3.2 Test Apparatus**

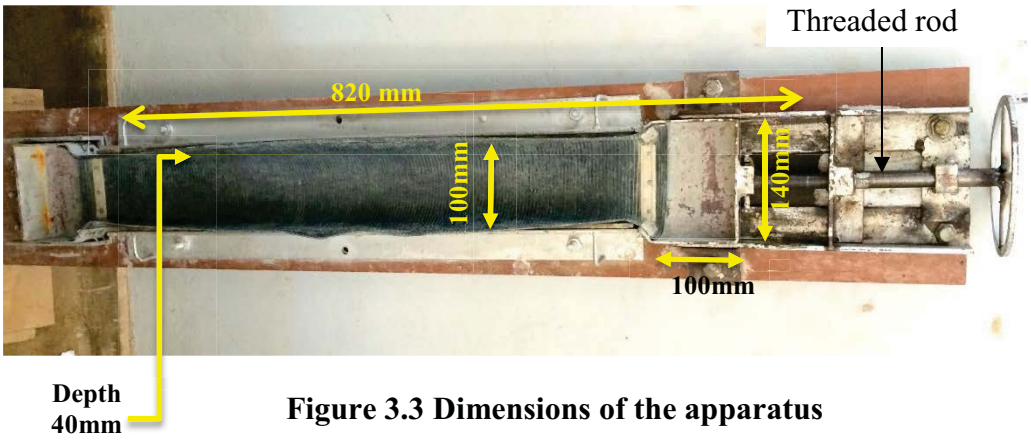


**Figure 3.3 Dimensions of the apparatus**

Rubber membrane connected to steel casings at both ends was fixed at one end and movable at the other end. Threaded rod where the movable end was connected can be pulled by rotating the wheel. Rubber membrane has ribs which can grip the concrete sample. Steel casing around the rubber membrane ensured it maintained its shape during the test. Perspex sheets had been placed between the steel frame and the rubber membrane to reduce friction. However, friction does not affect the results as only the local tensile strain on the concrete sample was measured.

**Figure 3.4 Test procedure**

As shown in the Figure 3.4, after compacting concrete in the rubber mould and placing the markers on top of it, the apparatus was placed under a steel frame. Special guides were marked in order to place the apparatus at the centre of the frame every time. On top of the steel frame, the camera was mounted. The wheel was rotated at a constant rate and images were taken from the camera. The strain application rate was 0.3 mm/s

and this was based on the literature review to give a realistic variation of strain capacities with time.

Before testing the actual concrete samples the test method has to be fine-tuned. In order to do so 1:5 cement: sand mortar mix was tested. Mix was prepared and poured to the rubber mould. Apparatus was placed on a vibrating table and vibrated until it was well compacted. Then markers were placed on top of it. Apparatus was placed under the tripod and strain was applied until cracks started to appear. Photos were taken and analysed. The strain distribution was satisfactory and peaks coincided with the cracks (See figure 3.6).

The important task at this stage was to derive the scale factor for the images taken (see Figure 3.5). Photos are taken from a stationary camera at the centre. Therefore the pixel length to actual length ratio changes towards the either ends.

No. of pixels representing 1cm at middle = 30 pixels

No. of pixels representing 1cm at the ends (40cm and -40cm) = 28 pixels

Scale factor at middle = 1

Scale factor at ends (40cm and -40 cm) = 30/28 = 1.07

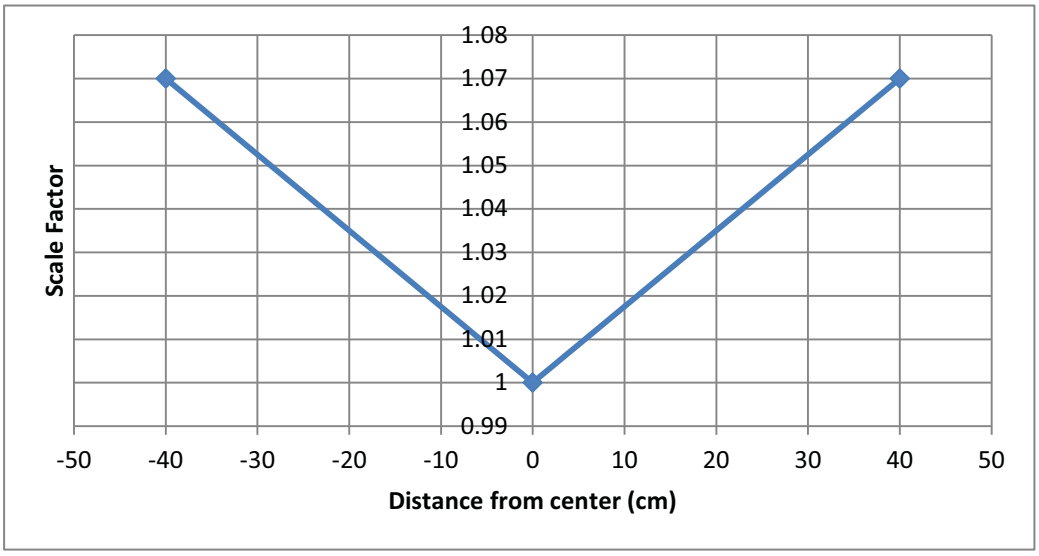


**Figure 3.5 Scale factor**

Tensile strain was calculated as follows. Pixels between adjacent markers were recorded at start and at the crack initiation point. Distance from centre to each marker was recorded by laying a steel measuring tape along the sample, thus the scale factor at each marker can be calculated.

$$Tensile\ Strain\ Capacity = \frac{(No.\ of\ pixels\ at\ failure \times scale\ factor) - (No.\ of\ pixesls\ at\ start\ \times scale\ factor)}{(No.\ of\ pixesls\ at\ start\ \times scale\ factor)}$$

Figure 3.6 shows the strain distribution over the sample length.

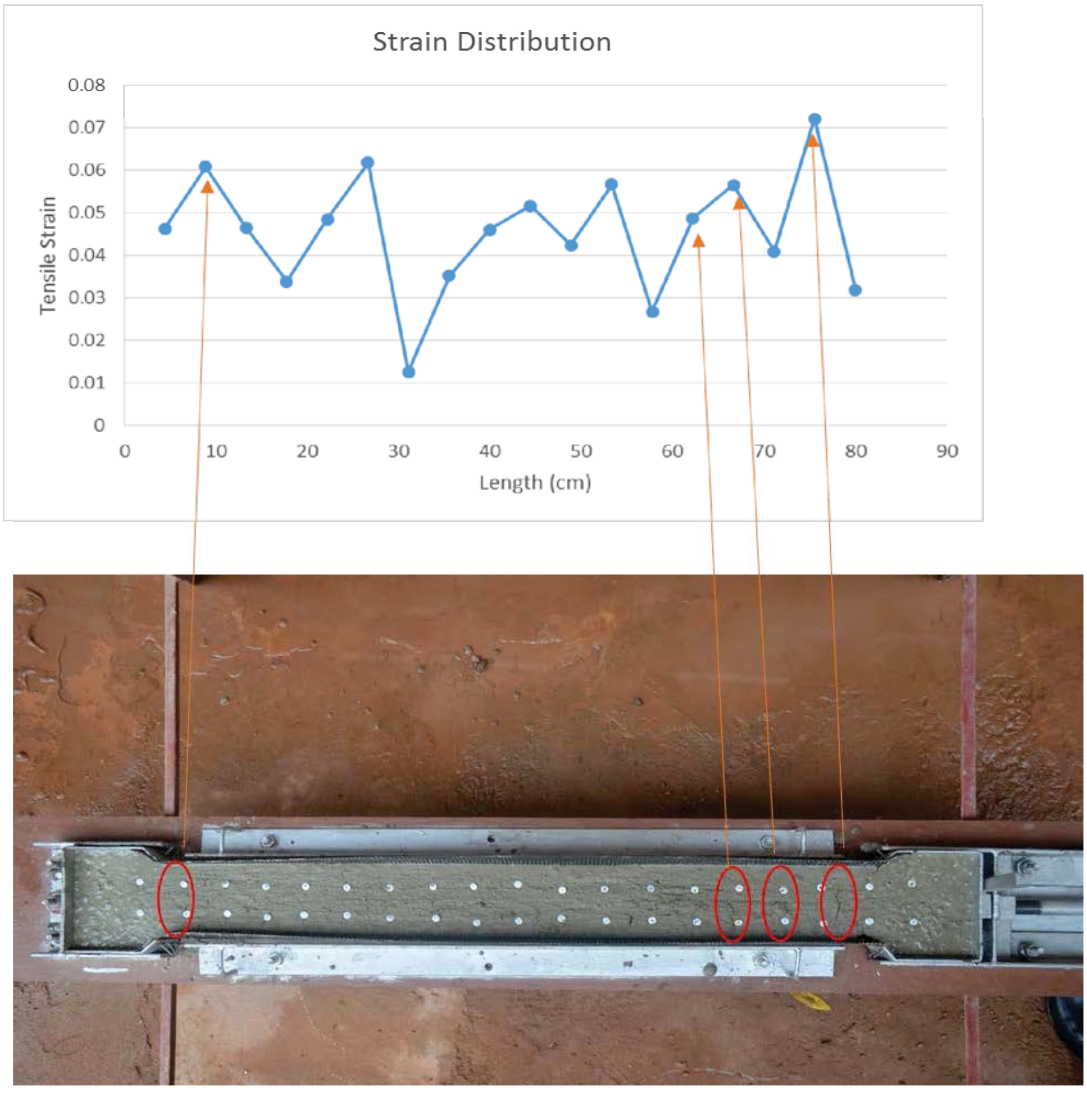


**Figure 3.6 Strain distribution along the sample**

### 3.3.1 Behavior of Markers

It was noted that there was a sudden peak in the strain distribution along the sample and the adjacent strain values were really low compared to that. The variation of the strain was drastically changing near the location of crack. To investigate the reason for that displacement of a marker with time starting from the beginning to crack initiation point was plotted. Figure 3.7 shows the results.

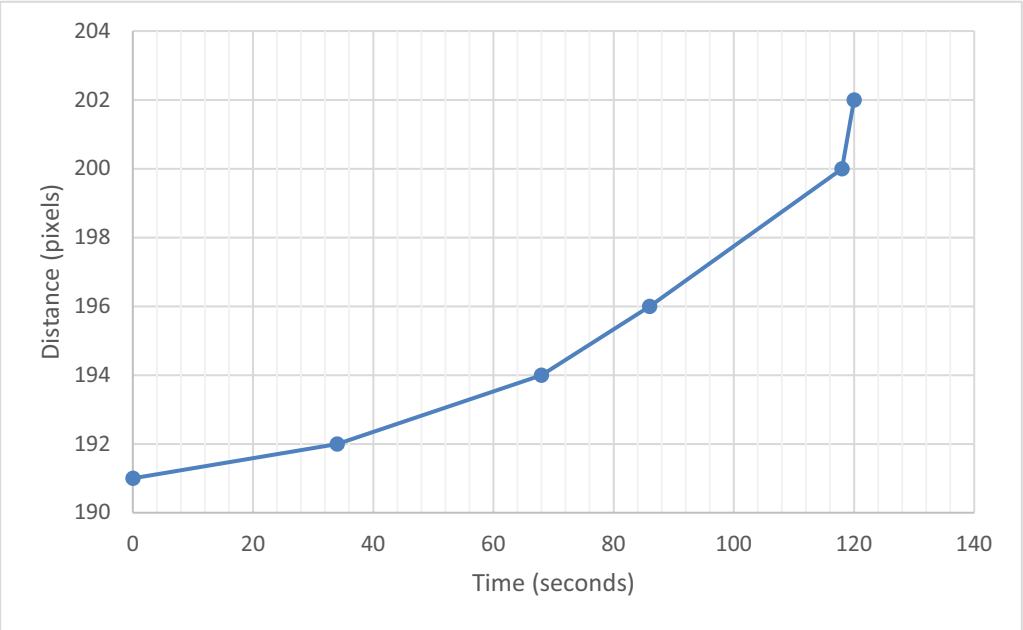


**Figure 3.7 Distance between two markers vs time**

This indicates that just before the cracking there is a sudden increase in the distance between two markers. That explains the sudden peak in the strain distribution plots. Regions adjacent to the crack which were not cracked do not deform that much as the applied strain is concentrated near the crack. Therefore the regions beside the crack has relatively low strain.

### 3.4 Selection of Materials and Mix Proportions

Objective of the research was to study the effect of cement type and type of fine aggregate on the tensile strain capacity. Therefore three common cement types used in Sri Lanka and two different fine aggregates were chosen. They are;

- Ordinary Portland Cement (OPC)
- Fly ash blended cement
- Portland Limestone Cement (PLC)
- River sand
- Manufactured Sand

DoE mix design method was used to determine the mix proportions. Cement type was varied keeping other parameters constant to find the influence of cement type. To find the influence of fine aggregates, river sand in the reference OPC mix was replaced by 20% and 50% by volume using manufactured sand. To find out the effect of mortar phase of concrete to strain capacity, the reference OPC mix proportion was used without coarse aggregate. Mixes were designed for a slump of 160mm and a characteristic strength of 30N/mm$^2$ (Grade 30).

**Table 3.1 Mix proportions (for 1m$^3$)**

| | **OPC** | **OPC + Fly Ash (20%)** | **PLC** | **MSand 20%** | **MSand 50%** | **Mortar Phase** |
|---|---|---|---|---|---|---|
| Coarse Aggregates (20mm) | 1059kg | 1059kg | 1059kg | 1059kg | 1059kg | - |
| Fine Aggregates | 706kg | 706kg | 706kg | RS – 144kg<br>MS –565kg | RS – 360kg<br>MS –353kg | 877kg |
| OPC | 410kg | 328kg | 410kg | 410kg | 410kg | 510kg |
| Fly Ash | - | 82kg | - | - | - | - |
| Water | 205kg | 205kg | 205kg | 205kg | 213kg | 255kg |
| W/C | 0.5 | 0.5 | 0.5 | 0.5 | 0.52 | 0.5 |
| Slump | 155mm | 140mm | 160mm | 150mm | 145mm | - |

## 3.5 Test Procedure

At the initial phase, the test was carried out to simulate the practical situation of placing concrete. One set of mixes were mixed in a mixing drum (whole quantity at once) and kept inside it (see Figure 3.10). The drum was closed to prevent evaporation. At every 10 minutes, concrete is agitated and taken out at the required time interval for the test. This will simulate concrete being kept inside an agitator before placing it (Method 1).

The other set of mixes were freshly prepared and placed inside the rubber mould of the apparatus soon after mixing. Concrete sample kept undisturbed until the test was carried out at the required time interval (Method 2) (see Figure 3.9). This was to simulate the normal shrinkage of concrete after it was placed. The same procedure was adapted to test the influence of fine aggregate type and mortar phase. Figure 3.8 illustrates the tests conducted.

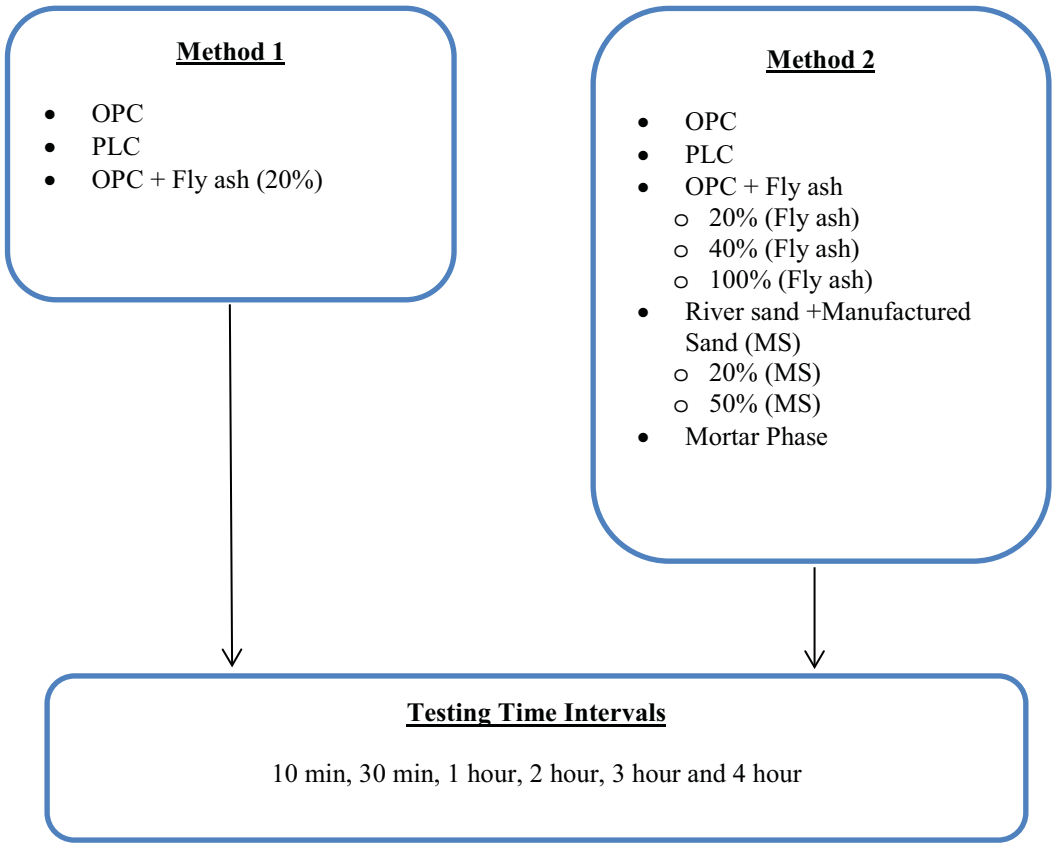


**Figure 3.8 Test matrix**

**Figure 3.10 Method 1 - Keeping the mix inside the mixer**

**Figure 3.9 Method 2 - Sample kept in the mould undisturbed**

The test was conducted as follows.

a) Apparatus was placed on the vibrating table.
b) Concrete was placed inside the rubber mould and vibrated for good compaction.
c) Markers were placed on the concrete surface along the longitudinal direction.
d) Apparatus was covered by polythene sheet and placed at the centre of the tripod.
e) A steel measuring tape was placed along the sample as a reference.
f) Strain was applied by rotating the wheel (at a rate of approximately 0.2 rps i.e. 0.3mm/s) until the cracks appear.
g) Photos were taken continuously from start to crack initiation point.


**Figure 3.11 A sample photo taken to measure strain**

**Figure 3.12 Taking photographs from top while applying strain**

## 3.6 Processing Images and Calculating Strain Capacity

Images were processed using Adobe Photoshop CS3. A grid line was created such that each square represent a pixel (see Figure 3.13). Number of pixels between adjacent markers was counted. Position of each marker was also recorded using the reference steel measuring tape placed along the sample. So the scale factor corresponding to each region between two adjacent markers can be calculated. Strain was calculated using the following equation and plotted along the sample length.

$$Tensile\ Strain\ Capacity = \frac{(No.of\ pixels\ at\ failure \times scale\ factor) - (No.of\ pixesls\ at\ start\ \times scale\ factor)}{(No.of\ pixesls\ at\ start\ \times scale\ factor)}$$

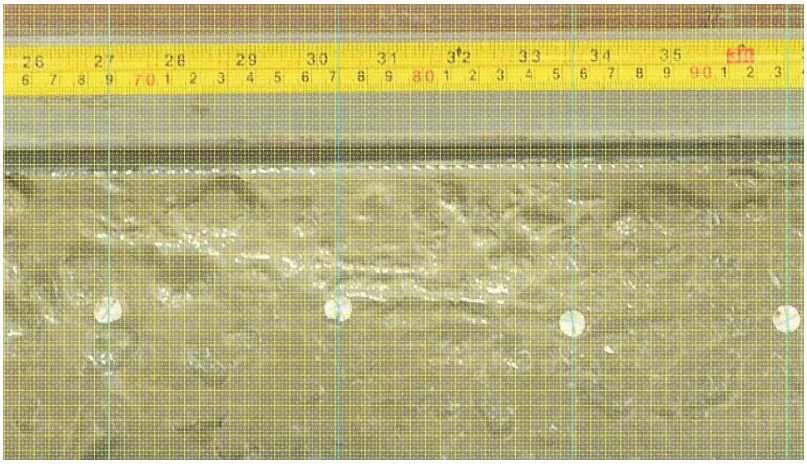

**Figure 3.13 Image used to calculate strain**

### 3.7 Test Results

Test was carried out according to two methods.

**Method 1**: Total quantity of concrete was mixed at once and a sample was taken from the mixer at the time of testing and then tested. The mixer was agitated at every 10 minutes for 2 minutes. OPC, Fly Ash blended and PLC cement types were tested according to this procedure.

**Method 2**: A freshly prepared concrete at each time interval was tested. OPC, Fly ash blended, PLC, mortar phase and effect of manufactured sand was tested according to this procedure.

Location where cracks initiate was identified from the images and the change in displacement at that location was measured using the image analysis described in 3.6. Local strain at the point of cracking was calculated using the measured displacements and expressed as the tensile strain capacity of fresh concrete at that time. Detailed calculations are shown in Appendix A and the variation of tensile strain capacities with time for different cement types and fine aggregate types are shown in the following figures (Fig. 3.14 to 3.18).

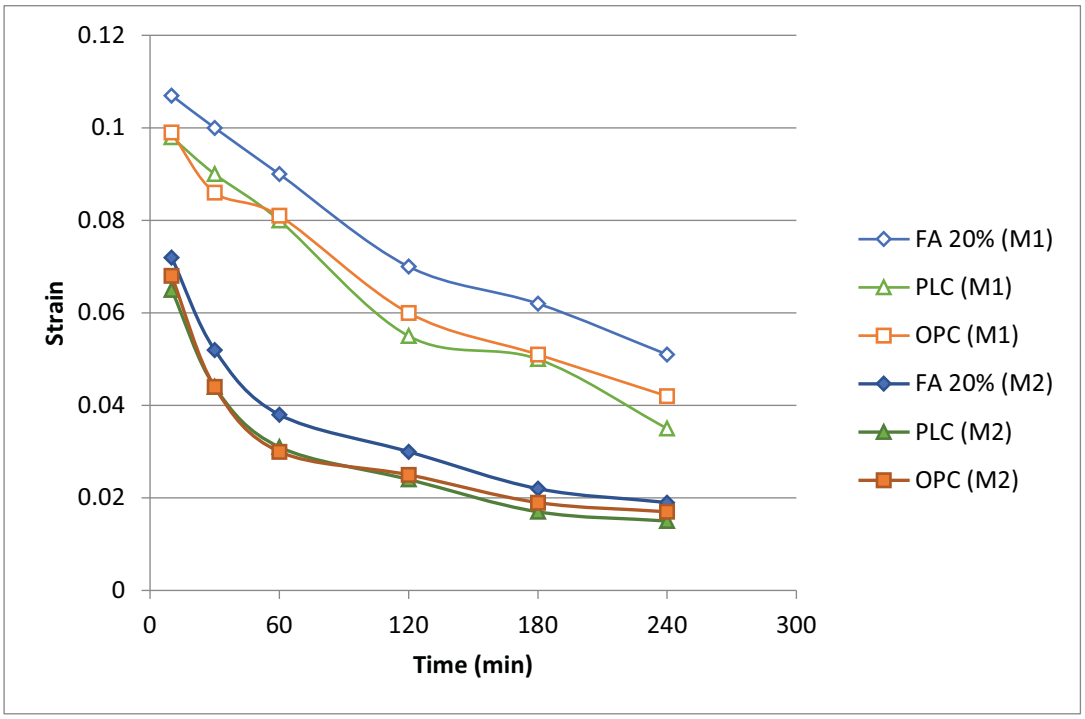


**Figure 3.14 Comparison of tensile strain capacities for two methods**

In Figure 3.14 strain capacities obtained from two methods for different cement types are compared. Strain capacities for all the cement types are higher for method 1 than method 2. The reason for this is due to delay in setting of concrete as a result of agitation at every 10 minutes in method 1. The test was performed in the plastic state and with agitation, concrete was bought back to semi-liquid phase. Therefore, the tensile strain capacities are comparatively high. As per in method 2 concrete is placed in the mould and kept undisturbed which allows concrete to stiffen and therefore the tensile strain capacity is low.

To compare the influence of cement type, tensile strain capacities obtained from method 2 were used (See figure 3.15). Rest of the tests were carried out using method 2 will be presented as it represents more closely the actual situation after placing concrete.

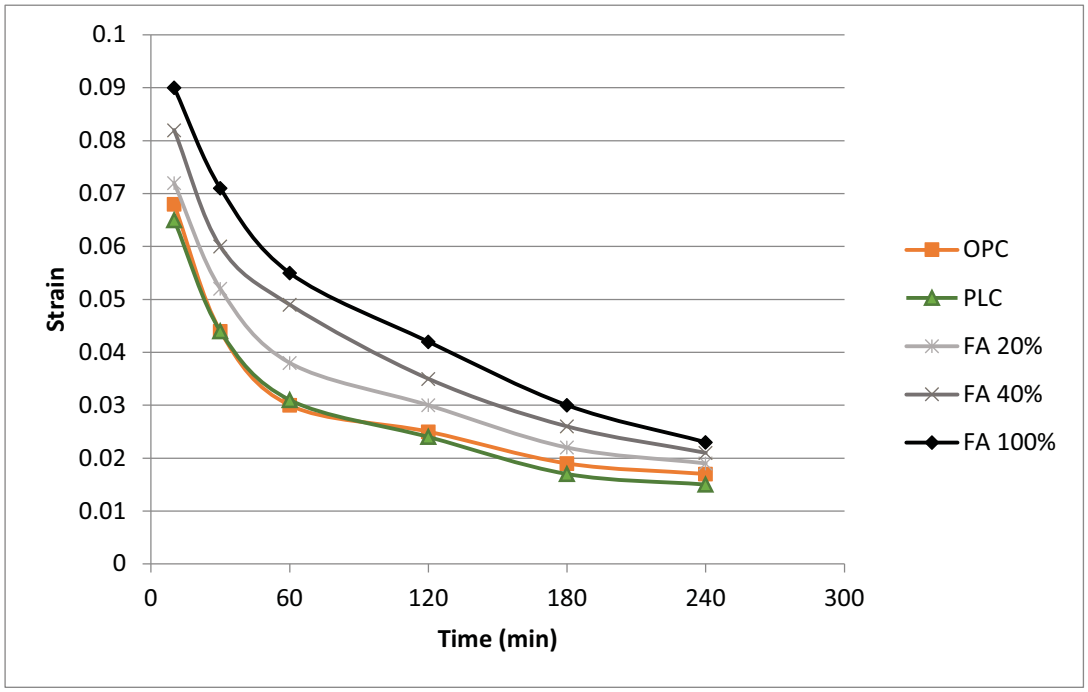


**Figure 3.15 Influence of cement type for tensile strain capacity**

In addition to 20% replacement of OPC with fly ash, two additional mixes were considered i.e. 40% and 100% fly ash replacement of OPC. Even though 100% replacement with fly ash will not get hardened, results of this mix helps to understand the influence of cement hydration on tensile strain capacity of fresh concrete. From the

results, it can be seen that there is no significant difference of tensile strain capacities of concrete with OPC and PLC. However, the concretes with fly ash blended cements are having higher tensile strain capacities than OPC and PLC. Also it can be seen that the tensile strain capacity increases with the increase of fly ash percentage. The reason could be the fineness of fly ash particles. As fly ash particles are finer than OPC particles it improves the cohesiveness (Mehta et al., 2013). Higher the cohesiveness of the mix more strain it can withstand before cracking.

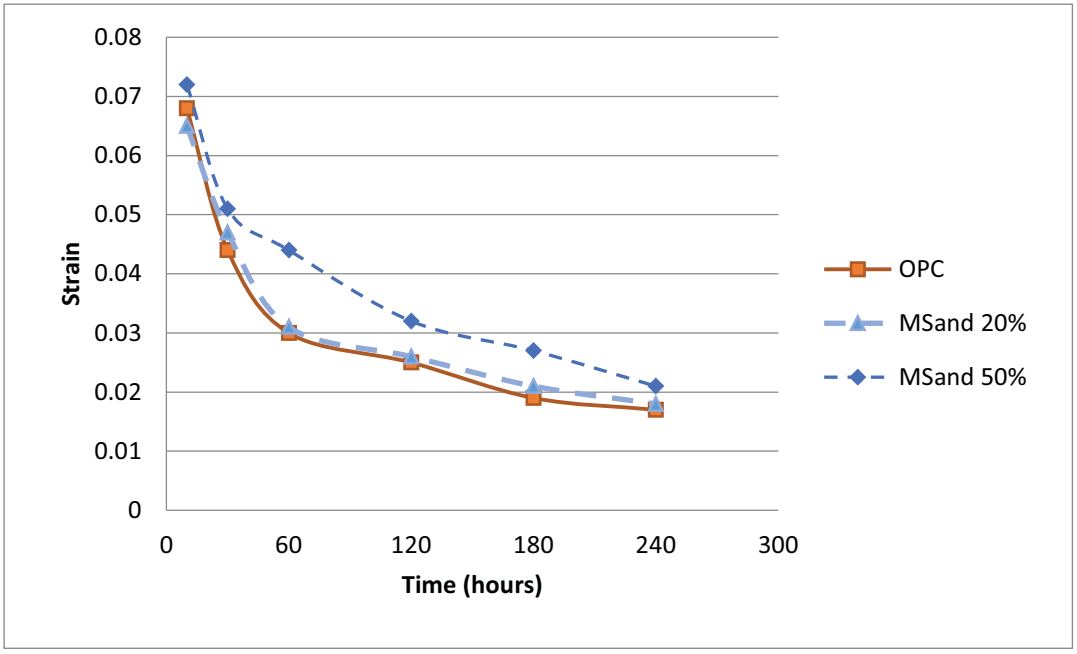


**Figure 3.16 Influence of fine aggregate type for tensile strain capacity**

Figure 3.16 shows the influence of fine aggregate type on the tensile strain capacity of fresh concrete. For the reference OPC mix normal river sand was used and it was replaced by 20% and 50% (by volume) using manufactured sand. A slight increase of strain capacity has been reported for the 20% replacement but a significant increase in strain capacity was reported when 50% of river sand was replaced with manufactured sand. Figure 3.17 shows particle size distribution of river sand and manufactured sand used in the test. It can be seen that manufactured sand is having more fines than river sand and this can be the reason for higher tensile strain capacity of concrete with

manufactured sand. This behaviour confirms that the tensile strain capacity of fresh concrete depends on the cohesiveness of the mix which can be as a result of fine particles.

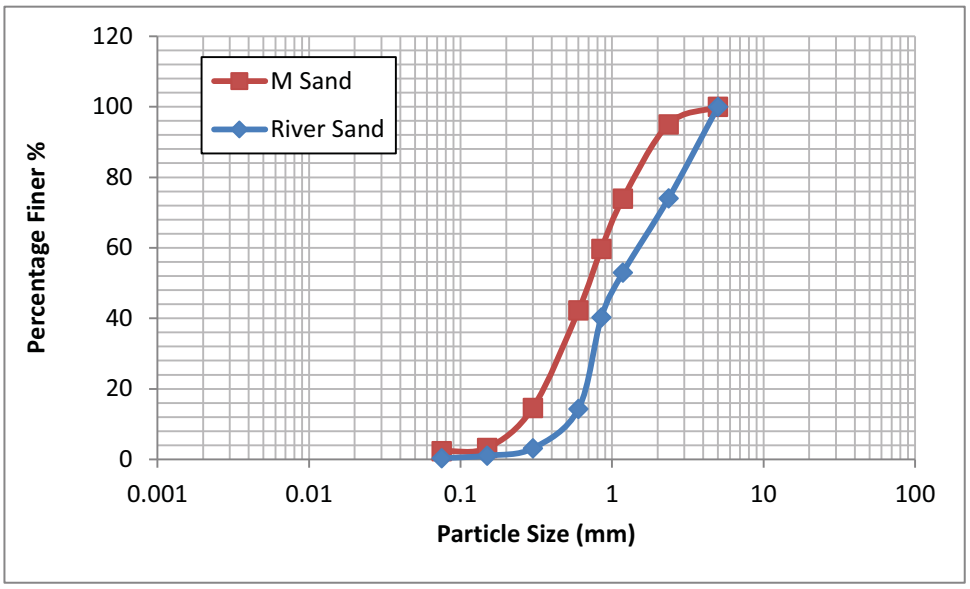


**Figure 3.17 Particle size distribution of fine aggregates**

Literature review suggested that plastic shrinkage behaviour is mainly governed by the mortar phase of concrete. (Slowik et al., 2008 and Roziere et al., 2015). To find out whether this observation is valid for the strain capacity as well it was decided to do the test for the mortar phase of the reference mix and compare it with strain capacities of concrete mix. Figure 3.18 shows the results obtained.

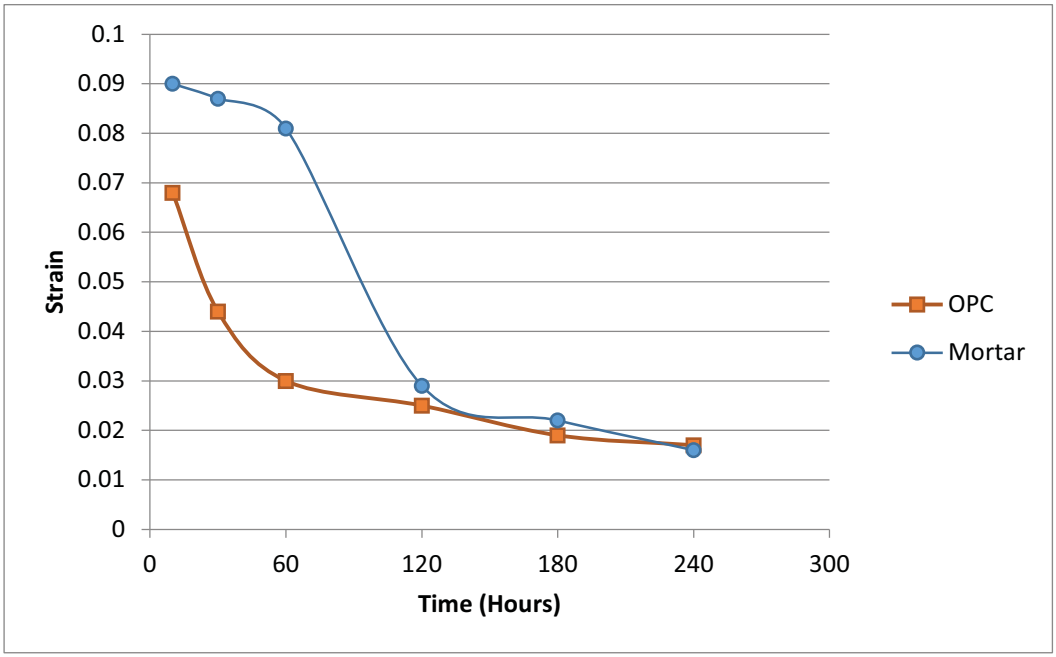


**Figure 3.18 Influence of mortar phase for tensile strain capacity**

Initially the strain capacity was significantly higher than that of the concrete but after 2 hours both concrete and mortar showed no significant difference in their tensile strain capacities. After 2 hours probably the mortar has reached its initial setting time and that may be the cause for the sudden drop of strain capacity. The results suggest that after initial setting time period, coarse aggregate has no influence to the tensile strain capacity thus it confirms that plastic shrinkage behaviour is governed by mortar phase of the concrete.

## 3.8 Summary

After studying the drawbacks of the previous test methods a novel test method was developed to measure the tensile strain capacity of fresh concrete. Images of the deformed free surface of fresh concrete samples were analyzed and the local strain at the cracking location was found. Using the test method developed, the influence of various factors such as cement type, mortar phase and type of fine aggregate on the tensile strain capacity of fresh concrete was studied. The results indicated that the strain capacity decreases non-linearly with time. It also revealed that replacement of OPC by fly ash increases the strain capacity where as OPC and PLC showed more or less the same strain capacities. Replacement of river sand by finer manufactured sand also increased the strain capacity which may be due to increase in cohesiveness of mix as a result of addition of fines. Furthermore, the influence of mortar phase was studied and it revealed that after the initial setting time, both mortar and concrete exhibits the same tensile strain capacities. This confirms the observations of previous studies that plastic shrinkage cracking is mainly governed by the mortar phase of concrete.

# 4 MODELING OF SHRINKAGE DEVELOPMENT

## 4.1 General

Bleeding and Evaporation are the two main factors which governs the plastic shrinkage in fresh concrete. Therefore, in order to model shrinkage development, bleeding and evaporation should be accurately modeled. After that, those two models can be incorporated to predict the volume loss in concrete which ultimately results in shrinkage strain. This chapter focuses on the techniques used to model bleeding and evaporation and verification of the accuracy of those models with experimental results from an independent test.

## 4.2 Modeling of Bleeding

Bleeding occurs due to the settlement of solid particles which causes upward displacement of water. Tan has proposed a bleeding model based on consolidation settlement and it is widely used to predict the amount of bleed water (Tan et al., 1987). Kwak has further simplified the method to be used for specific boundary conditions and he has verified the accuracy of the model using the experimental results of several researches (Kwak et al., 2006). Hence this model was used to model bleeding for the experiment conducted by Slowik regarding strain development in fresh concrete (Slowik et al., 2008). Details of the bleeding model can be found in chapter 02 and only the essential content will be discussed in this chapter.

Governing equation for the bleeding model is given by (see equation 4.1).

$$\frac{\beta K_0}{\gamma_w}\frac{\partial^2 e(z,t)}{\partial z^2} = \frac{\partial e(z,t)}{\partial t} \quad \text{……..….(4.1)}$$

Where,

β and $K_0$ - Constants determined from the mix proportions of the concrete

$\gamma_w$ - Unit weight of water

*e* - Water to solid ratios by volume at time t

z - Height of solids.

Equation 4.1 was simplified for a particular boundary condition as shown in Figure 4.1.

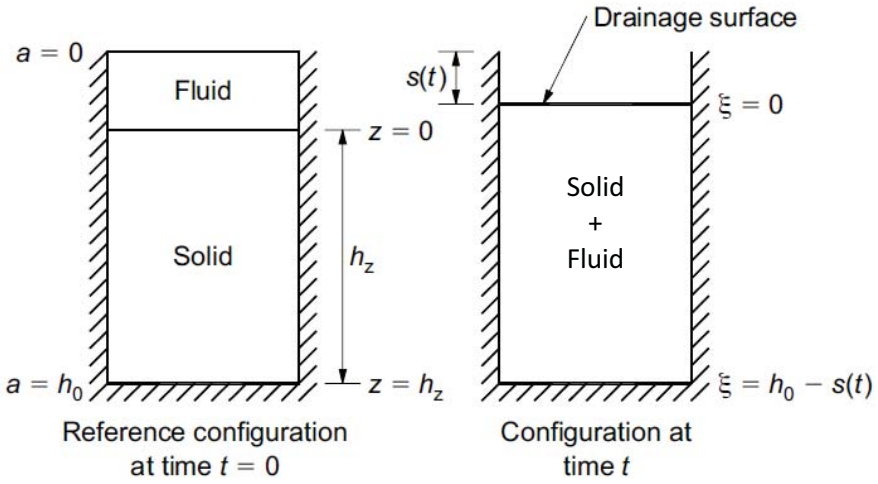


**Figure 4.1 Simplified bleeding model (Tan et al, 1987)**

Amount of bleeding was equivalent to the surface settlement s(t) and is calculated by equation 4.2.

$$s(t) = h_0 - \int_0^{h_z} [1 + e(z,t)]dz \quad \text{.....(4.2)}$$

The finite difference method was used to determine the void ratio *e(z,t)* at time t as follows.

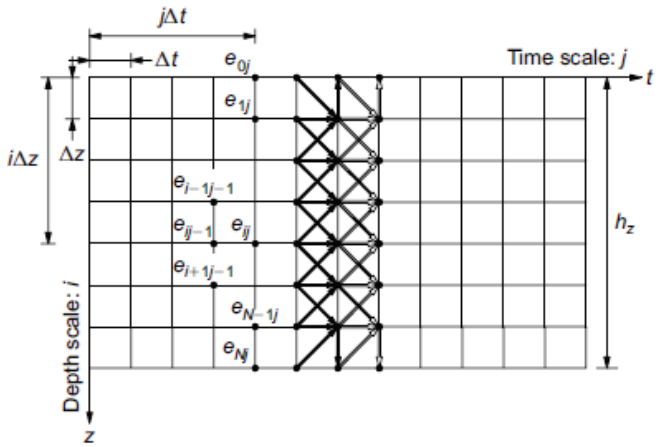


**Figure 4.2 Finite difference element idealization for void ratio**

Corresponding governing equation and boundary conditions are represented by equations 4.3 and 4.4.

$$e_{i,j+1} = e_{i,j} + \frac{\beta K_o \Delta t}{\gamma_w (\Delta z)^2}(e_{i+1,j} - 2e_{i,j} + e_{i-1,j}) \quad \text{.....(4.3)}$$

$$e_{i,0} = e_o,\ e_{0,j} = e_o,\ e_{N,j} = e_{N-1,j} + \frac{\gamma_w - \gamma_s}{\beta}\Delta z \quad \text{.....(4.4)}$$

Where,

$e_{i,j}$ – void ratio of cement paste at the *i*th location and the *j*th time

$\Delta z$ – element length along the depth axis

$\Delta t$ – time step

For the boundary conditions shown in Figure 4.2 following parameters were used.

a) At time t = 0, $e(z,0) = e_0$ (Initial water to solid ratio was taken as $e_0$ )
b) At the top surface z = 0, $e(0,t) = e_0$ (At any given time t, water to solid ratio at the top surface was taken as $e_0$ because there is a thin layer of water formed on the top surface)
c) At the bottom impervious surface z = $h_z$, $de/dz=(\gamma_w-\gamma_s)/\beta$ where $\gamma_s$ unit weight of cement.

In addition, to obtain a general solution using the finite difference method, the stability condition for the time step and element length, the following condition should be satisfied (Eq. 4.5).

$$\frac{\Delta t}{(\Delta z)^2} < \frac{\gamma_w}{2\beta K_0} \qquad \text{……..…..(4.5)}$$

In order to calculate $\beta$ and $K_0$ factors which depend on the mix proportion, Kwak has proposed regression formulas (Eq. 4.6 and 4.7) after comparing the model with numerous independent experimental results (Kwak, 2006)

$$K_0 = K_{0,ref}.\lambda_{K_o,w/c}.\lambda_{K_o,W}.\lambda_{K_o,s/a}.\lambda_{K_o,H} \qquad \text{…..…...….(4.6)}$$

$$\beta = \beta_{ref}.\lambda_{\beta,w/c}.\lambda_{\beta,W}.\lambda_{\beta,s/a}.\lambda_{\beta,H} \qquad \text{…..……(4.7)}$$

Where,

$K_{0,ref}$ and $\beta_{ref}$ - Constants corresponding to the reference mix. $K_{0,ref}$= 1.274 x $10^{-5}$ m/min and $\beta_{ref}$ – 1.295 x $10^4$ kgf/$m^2$

$\lambda_{Ko,w/c}$ and $\lambda_{\beta,w/c}$ – Regression coefficient corresponding to water/cement ratio (w/c)

$\lambda_{Ko,W}$ and $\lambda_{\beta,W}$ – Regression coefficient corresponding to unit water content(W)

$\lambda_{Ko,s/a}$ and $\lambda_{\beta,s/a}$ – Regression coefficient corresponding to sand to aggregate ratio (s/a)

$\lambda_{Ko,H}$ and $\lambda_{\beta,H}$ – Regression coefficient corresponding to depth of the concrete(H)

The above bleeding model was used to predict the bleeding bahviour for the experiment conducted by Slowik (Slowik et al., 2008). The following mix proportion was used in the experiment and $e_0$ and sand to coarse aggregate ratio (s/a) was calculated and shown in Table 4.1.

**Table 4.1 Mix proportion used by Slowik (Slowik et al., 2008)**

| | |
|---|---|
| Cement CEM I 32.5R (kg/m$^3$) | 440 |
| Water (kg/m$^3$) | 180 |
| Fine aggregates (kg/m$^3$) | 614 |
| Coarse aggregates (kg/m$^3$) | 1117 |
| W/B | 0.41 |
| Specific gravity of Cement | 3.1 |
| Specific gravity of aggregates | 2.63 |
| $e_0$ (at t = 0) | 0.225 |
| sand/aggregate (by volume) | 0.355 |

Sample size considered in the experiment was 30cm x 30cm x 6cm. Corresponding regression coefficients were calculated using the graphs shown in figure 2.6 to 2.9 and given in Table 4.2.

**Table 4.2 Regression coefficients**

| Factor | $\lambda_{K_0}$ | $\lambda_\beta$ |
|---|---|---|
| Water / cement ratio (w/c) | 0.5 | 2.2 |
| Unit water content (W) | 1.2 | 0.8 |
| Sand/Aggregate ratio (s/a) | 2.2 | 0.5 |
| Depth (H) | 0.1 | 0.3 |

Using the above regression coefficient values and reference constants, $K_0$ and $\beta$ for the mix was calculated as;

$K_0 = 1.682 \times 10^{-6}\ m/min$

$\beta = 3.419 \times 10^3\ kgf/m^2$

A time step (Δt) of 2min and a element length (Δz) of 1cm along the depth was used in finite difference model to predict the bleeding behavior. Details are given in Appendix B. Figure 4.3 shows the amount of bleeding (in mm) with time and figure.

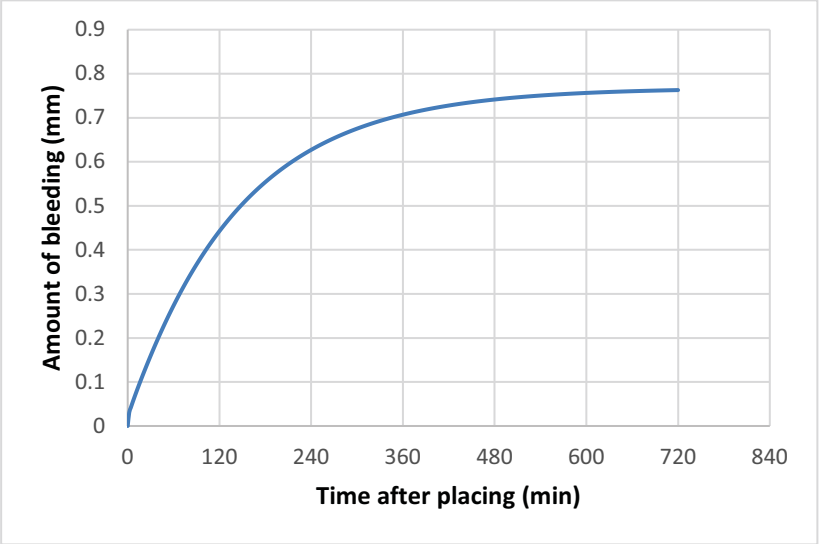


**Figure 4.3 Modelled bleeding behaviour for experiment by Slowik**

## 4.3 Modeling of Evaporation

Evaporation rate can be determined using the ACI monograph (see figure 2.10) for a given atmospheric temperature, relative humidity, concrete surface temperature and wind velocity. In the experiment, mass loss of water due to evaporation was measured (see figure 4.4) and based on that the evaporation rate was calculated as 0.4 kg/m$^2$/h.

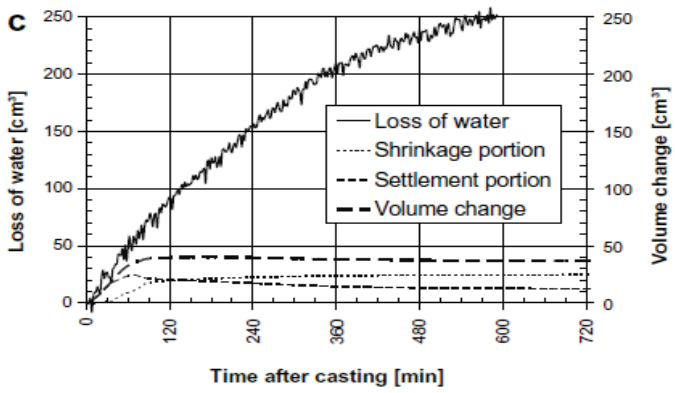


**Figure 4.4 Measured mass loss of water for the experiment by Slowik**

Assuming a constant evaporation rate ;

Loss of water for 4 hrs = 150 cm$^3$
Loss of water per hour
from 30cm x 30cm surface = 37.5 cm$^3$
Loss of water per hour
from a unit area = $\frac{(37.5 \times 10^{-6} \times 10^3 \text{ kg})}{(0.3 \times 0.3 \text{ m}^2)}$
Evaporation rate = 0.4 kg/m$^2$/h

## 4.4 Modeling of Plastic Shrinkage

### 4.4.1 Initiation time of drying and Rate of drying

Bleed rate and evaporation rate can be combined to determine the critical point at which the bleeding and evaporation are balanced, i.e. drying point (See Figure 4.5). After that point, the difference between the amount of water evaporated and the amount of bleed water is taken as the volume loss from fresh concrete which causes it to shrink.

From the analytical model, it can be seen (Figure 4.5) that the drying begins approximately at 30min after casting. Drying point predicted by the model matches with the experimental data as the shrinkage is zero up to 30 min and then gradually starts to increase (Figure 4.6).

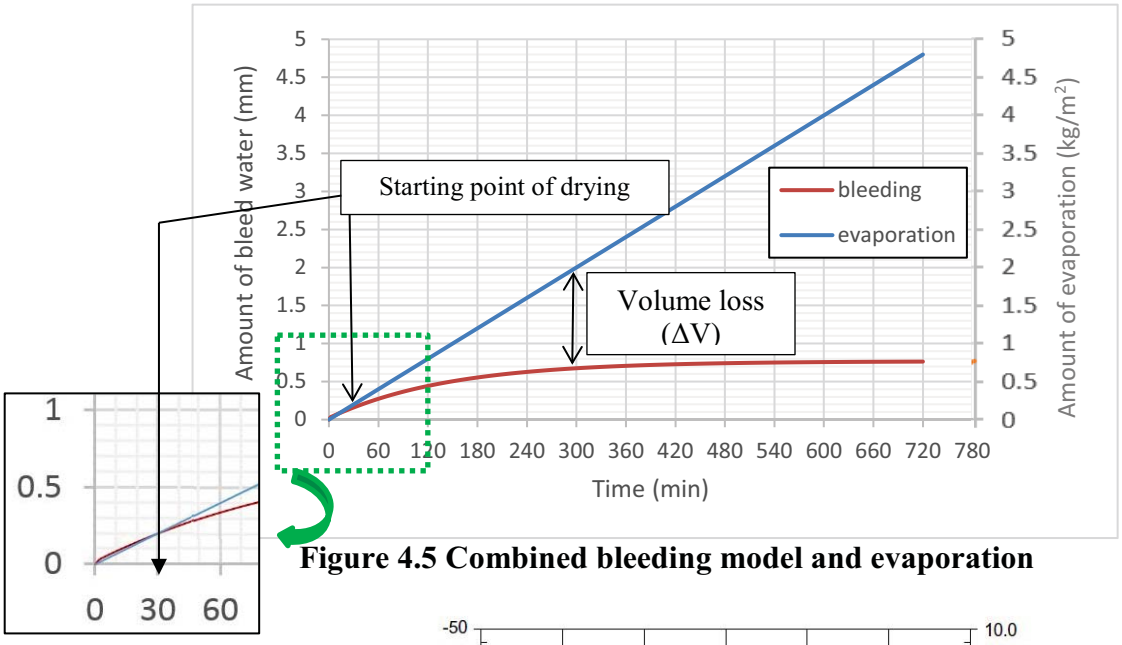


**Figure 4.5 Combined bleeding model and evaporation**

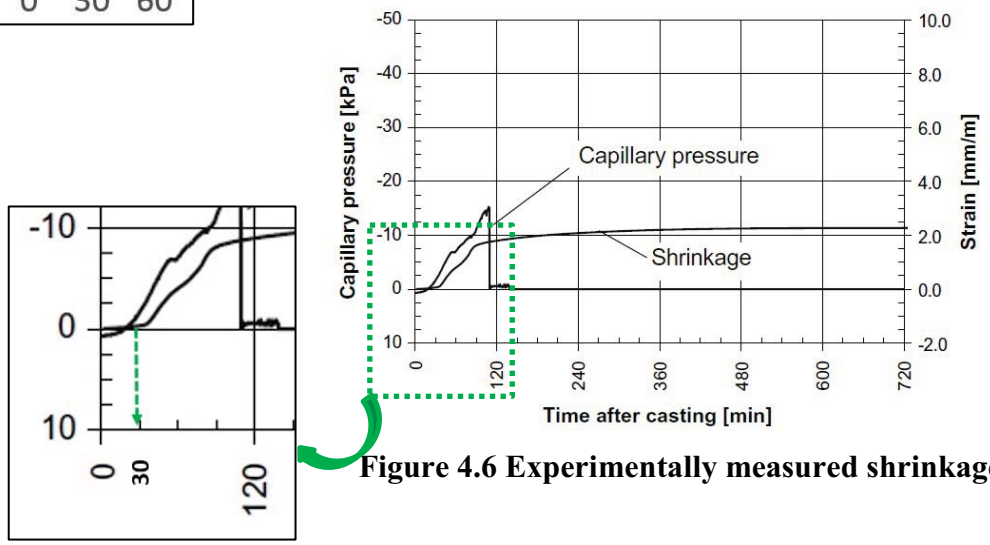


**Figure 4.6 Experimentally measured shrinkage**

### 4.4.2 Finite element modeling of plastic shrinkage

At the point of drying, the e value (volume of water to volume of solid ratio) can be obtained from the bleeding model for number of layers across the depth. In the current study, the sample (6cm in height) used in the experiment was divided into 1cm thick layers and for each layer, the corresponding e value was calculated from the analytical model for bleeding. Hence the amount of water retained at each layer at the time when drying starts is known. For each time interval after the drying point, corresponding volume loss of water from the whole sample can be calculated from the difference between total evaporation and total bleeding (Fig. 4.5 and Table 4.3). Volume loss for each layer is proportionate to the percentage of water retained in each layer. The rationale behind the proposed shrinkage pattern is, higher the water content it has more capillary pores and they promote more evaporation. The top most layer has the highest percentage of water whereas the bottom most layer has the lowest. Therefore the relative shrinkage of the top layer is higher than the adjacent layer below it which has lower water content. This explanation matches the observations regarding plastic shrinkage mechanism (Radocea, 1994).

**Table 4.3 Calculated volumetric contraction**

| | t = 30 min | t=60 min | t=90 min |
|---|---|---|---|
| Total evaporation (kg/m2) | 0.2 | 0.4 | 0.6 |
| Total bleed volume (kg/m2) | 0.2 | 0.28 | 0.37 |
| Total contraction (kg/m2) | 0 | 0.12 | 0.23 |
| contraction for Δt (kg/m2) | 0 | 0.12 | 0.11 |
| contraction for Δt (mm3) | - | 10800 | 9900 |

**Table 4.4 Volume loss across the depth from 30 min to 60 min**

| Layers across the depth (cm) | top | *e* at t= 30 min | % of water | porosity | volume of water (mm3) | Volume loss (mm3) ; up to 60min | Temp. difference ($^0$C) | Thermal coefficient of expansion (α) |
|---|---|---|---|---|---|---|---|---|
| | 1 | 0.225 | 16.944 | 0.184 | 165306.1 | 1829.95 | 10.00 | 2.033E-04 |
| | 2 | 0.2247657 | 16.926 | 0.184 | 165165.6 | 1828.05 | 10.00 | 2.031E-04 |
| | 3 | 0.2241247 | 16.878 | 0.183 | 164780.8 | 1822.83 | 10.00 | 2.025E-04 |
| | 4 | 0.2224393 | 16.751 | 0.182 | 163767.2 | 1809.12 | 10.00 | 2.010E-04 |
| | 5 | 0.2188585 | 16.481 | 0.180 | 161604.2 | 1780.00 | 10.00 | 1.978E-04 |
| | 6 | 0.2127163 | 16.019 | 0.175 | 157864.4 | 1730.05 | 10.00 | 1.922E-04 |
| | bottom | | | | | Σ = 10800 | | |

**Table 4.5 Volume loss across the depth from 60 min to 90 min**

| Layers across the depth (cm) | top | *e* at t= 60 min | % of water | porosity | volume of water (mm3) | Volume loss (mm3) ; up to 90min | Temp. difference ($^0$C) | Thermal coefficient of expansion (α) |
|---|---|---|---|---|---|---|---|---|
| | 1 | 0.22196 | 16.943 | 0.182 | 163476.2 | 1677.32 | 9.17 | 2.033E-04 |
| | 2 | 0.22173 | 16.925 | 0.181 | 163337.5 | 1675.58 | 9.17 | 2.031E-04 |
| | 3 | 0.22110 | 16.877 | 0.181 | 162957.9 | 1670.83 | 9.17 | 2.025E-04 |
| | 4 | 0.21944 | 16.751 | 0.180 | 161958.0 | 1658.33 | 9.17 | 2.010E-04 |
| | 5 | 0.21593 | 16.482 | 0.178 | 159824.2 | 1631.76 | 9.17 | 1.978E-04 |
| | 6 | 0.20990 | 16.022 | 0.173 | 156134.3 | 1586.18 | 9.17 | 1.922E-04 |
| | bottom | | | | | Σ = 9900 | | |

At the starting point of drying (t=30min) the variation of e across the depth can be obtained from the bleeding model. At t= 60 min, the variation of e was calculated by reducing the loss of water from each layer for a period of 30 minutes (from 30 min to 60min). For each time interval, the corresponding volume loss (ΔV) for each layer was converted into a thermal contraction according to the equation 4.7(Table 4.5 & 4.6).

$$\Delta V = V_0 . \alpha . \Delta\theta \quad \text{.....(4.7)}$$

$\Delta V$ – Volume change

$V_0$ – Initial volume

$\alpha$ – Coefficient of thermal contraction

$\Delta\theta$ – Temperature difference

Finite element software Abaqus was used to model the shrinkage development. A 3-D deformable element having a size of 30cm x 30cm x 6cm (to match the sample size of the experiment as shown in Figure 4.7) was divided into 6 layers. Each layer was assigned with a thermal coefficient of contraction obtained from Table 4.4 and 4.5. After assigning the boundary conditions to match with the experiment (top surface kept un-restrained and other surfaces restrained) the whole model was subjected to a temperature drop of $\Delta\theta$ value as calculated in Table 4.4 and 4.5. This will result in a contraction which will simulate the shrinkage that will occur due to the loss of moisture. For the modeling purposes the input elastic modulus (E) was varied from 0.2

GPa to 20 GPa to simulate the fresh concrete and the change in output strain values were negligible.

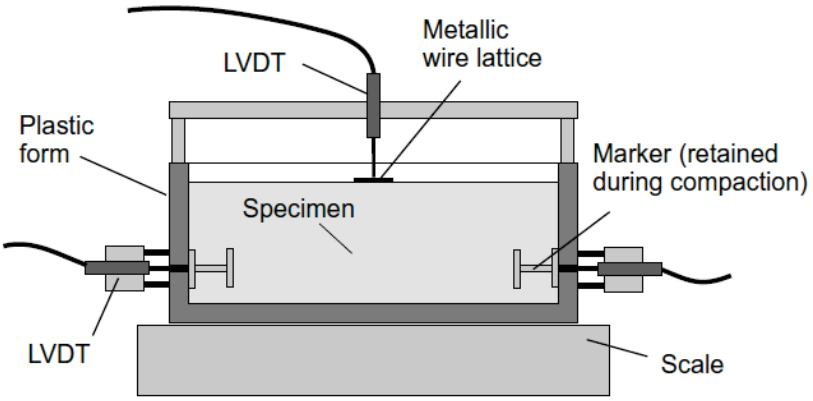


**Figure 4.7 Experimental set-up used by Slowik (Slowik et al., 2008)**

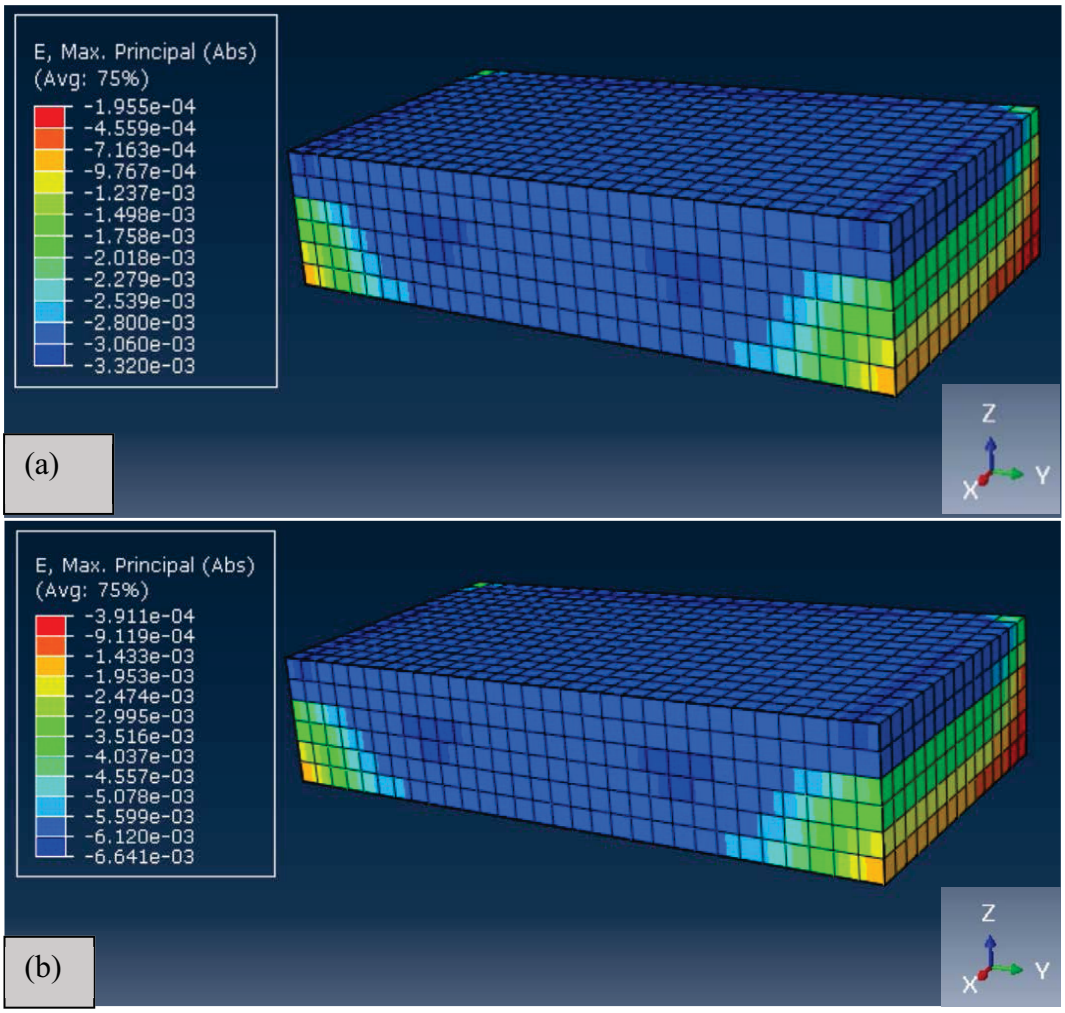


**Figure 4.8 Results of the FE analysis – Volumetric strain across the depth at the middle; (a) at 60 min and (b) at 90 min**

Figure 4.8 shows the output of the FE model, the cross-sectional view across the depth along the middle of the sample(x = 15cm). Average volumetric strain was obtained at z = 1 cm (As LVDTs were placed at that location) at time t=30 min and t=60 min are 0.0027 and 0.0057 respectively (Figure 4.8). Tensile strain variation across the sample depth can be clearly identified from the analytical results (Fig. 4.8) where the average tensile strain at top exposed layer is the highest and it gradually decreases as it goes down the sample depth. Strain contours are shown in Figure 4.8.

In the experiment, horizontal shrinkage was measured at the bottom of the sample. (At a depth of 5-6 cm). In the FE model, 3-D solid deformable elements were used hence the output contains the volumetric strain. These volumetric strains were converted to equivalent horizontal strains to compare with the experimental data. As seen in Figure 4.9. , the modeled shrinkage strains are very much similar to the measured shrinkage strains at time t = 60 min and t = 90 min.

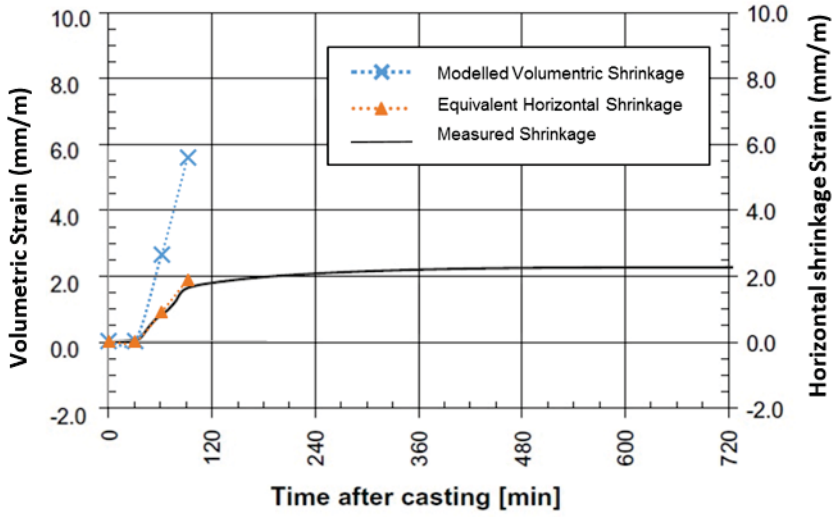


**Figure 4.9 Analytical results from the FE model and the measured shrinkage**

However after 90 min, the measured shrinkage strain reaches a limiting value. The rate of shrinkage decreases drastically and the reason behind this phenomenon can be the sudden drop of capillary pressure after it has reached its maximum value which disturbs the formation of continuous capillary pores thus preventing further shrinkage (see Fig. 4.6). Further investigations were carried out to accurately identify this limiting

condition. To limit the shrinkage strain at this limiting value, the maximum capillary pressure and the time taken to reach that pressure should be identified.

After analyzing the experimental results, Slowik has found that the maximum capillary pressure values (named as 'air entry value') for cement paste and concrete to be in the range between -10kPa and -45kPa whereas for fly ash it is in the range between -30kPa and -65kPa (Slowik et al., 2008). To find out the rate of capillary pressure development, the experimental results of Slowik and Hammer were considered (Slowik et al., 2008 and Hammer, 2007). Capillary pressure develops as a result of drying of the concrete surface. Therefore the aim was to find out a relationship between evaporation rate and the capillary pressure development rate. Findings are presented in a form of graph in Figure 4.10.

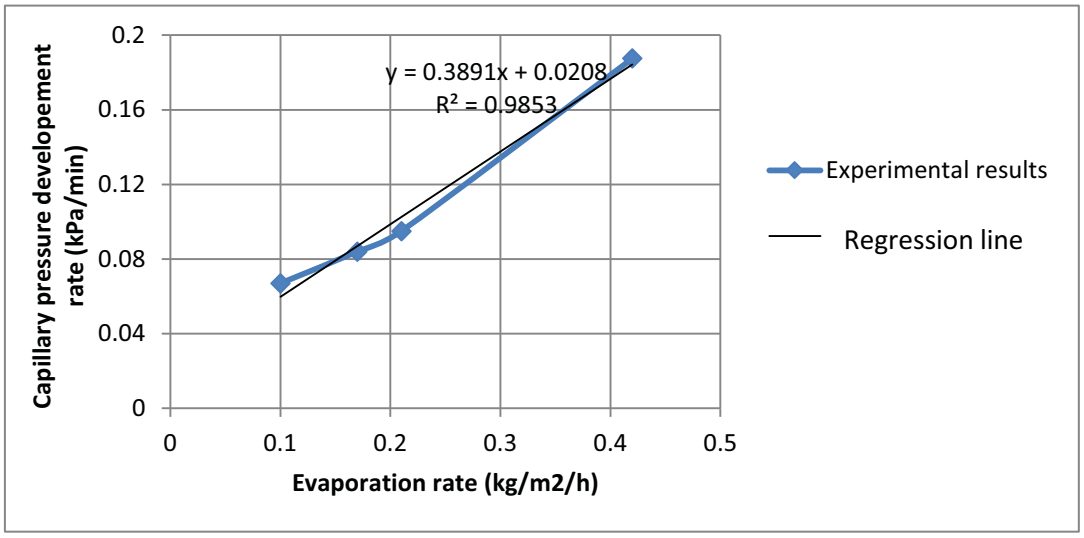


**Figure 4.10 Relationship between capillary pressure development and evaporation rate**

Based on Figure 4.10, time period for the capillary pressure in the above experiment to reach the upper and lower limits were estimated as 90 min and 270min (see Figure 4.11).

Evaporation rate = 0.4 kg/m$^2$/h

Capillary pressure development rate = 0.18 kPa/min ; From Fig. 4.1

Time taken to achieve a capillary pressure of -10kPa ($t_1$) = 10/0.18 = 56 min

Time taken to achieve a capillary pressure of -45kPa ($t_2$) = 45/0.18 = 250 min

$T_1$ = Drying initiation time + $t_1$ = 30 + 56 = 86 min ≈ 90 min

$T_2$ = Drying initiation time + $t_2$ = 30 + 250 = 270 min

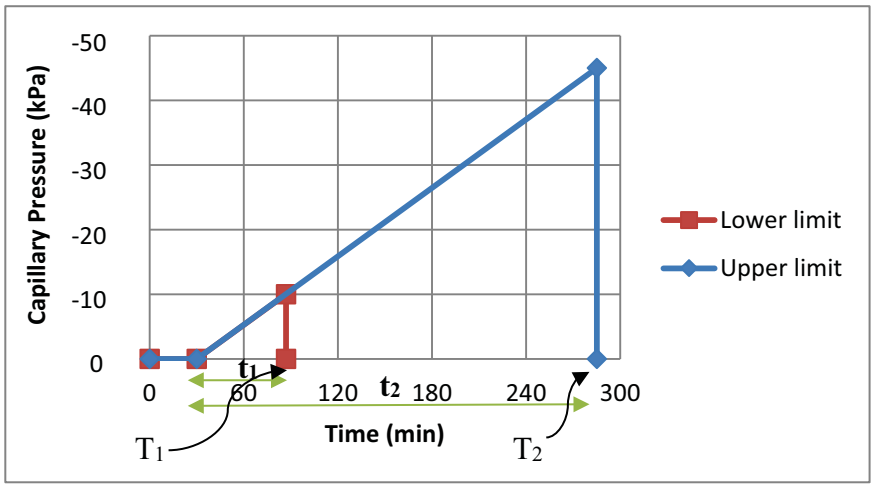


**Figure 4.11 Upper and Lower limits of capillary pressure**

However, in the experiment, the maximum capillary pressure measured was -15kPa and it has reached that value 110 minutes after casting (see Figure 4.6). Using the upper and lower limits, the finite element simulation was stopped at corresponding times and the results are shown in Figure 4.12. It is evident that the limiting value of shrinkage cannot be modeled exactly as measured because the exact time at which capillary pressure drops cannot be determined without measuring it. However, based on the two limits of capillary pressure proposed in the literature, two limiting values for shrinkage can be specified.

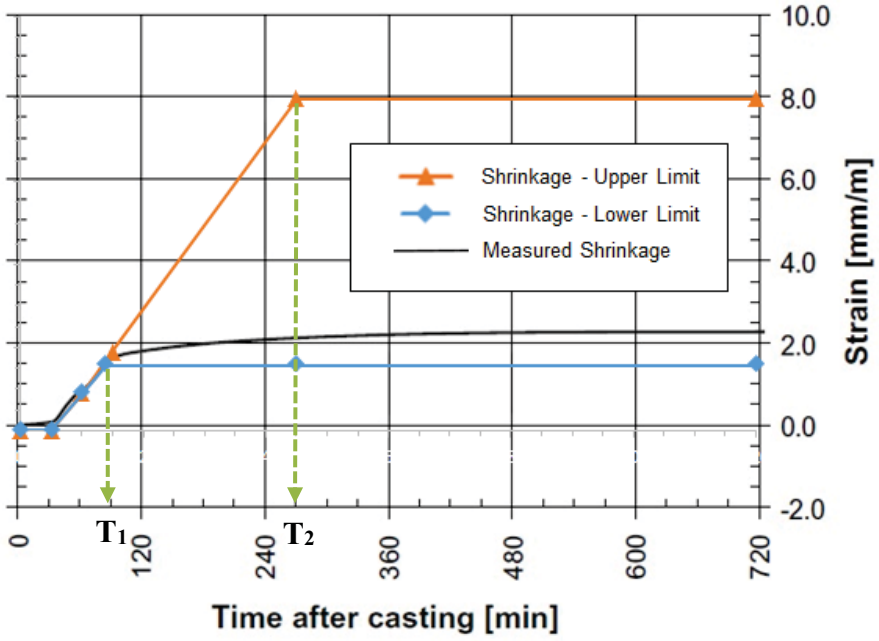


**Figure 4.12 Calculated shrinkage strain (upper and lower limits) with measured shrinkage strain**

## 4.5 Summary

Bleeding and Evaporation are the key factors governing the plastic shrinkage. In order to model shrinkage development in fresh concrete, these two parameters were modeled initially. Model proposed by Tan et al and simplified by Kwak et al was used to model bleeding while ACI nomograph was used to determine the evaporation rate. An independent research carried out by Slowik et al was used to verify the models. After modeling, bleeding and evaporation models are combined to find out the starting point of drying and the successive volume loss of water after that point. Corresponding volume loss was incorporated in a finite element model which was created using FE software Abaqus and the developed strain was predicted using the model. Comparisons of the modeled results with the experimentally measured strain revealed that they were very much similar. However, the strain reached a limiting value as the capillary pressure dropped after reaching its maximum value. Further investigations were done on the capillary pressure development in fresh concrete and ultimately an upper and lower limit for the limiting value of strain was proposed based on the findings. The crack initiation lies between these two limits.

# 5 RISK OF PLASTIC SHRINKAGE CRACKING

## 5.1 General

Having experimentally obtained the tensile strain capacities for different concrete mixes it was decided to investigate the influence of fly ash on the risk of plastic shrinkage cracking. For this purpose, strain development of fresh concrete was modeled for concrete made with OPC and 20% replacement of OPC with fly ash.

## 5.2 Bleeding Models for concrete with OPC and Fly ash blended cement

Bleeding model proposed by Tan et al. and Kwak et al was used to model the bleeding behavior as explained in chapter 04. However, it should be mentioned that the bleeding model does not incorporate a factor to account for the change in cement matrix due the replacement from fly ash. Therefore it was decided to measure the amount of bleeding first and then represent that behavior using the bleeding model. Figure 5.1 shows the amount of bleeding measured according to ASTM C232.

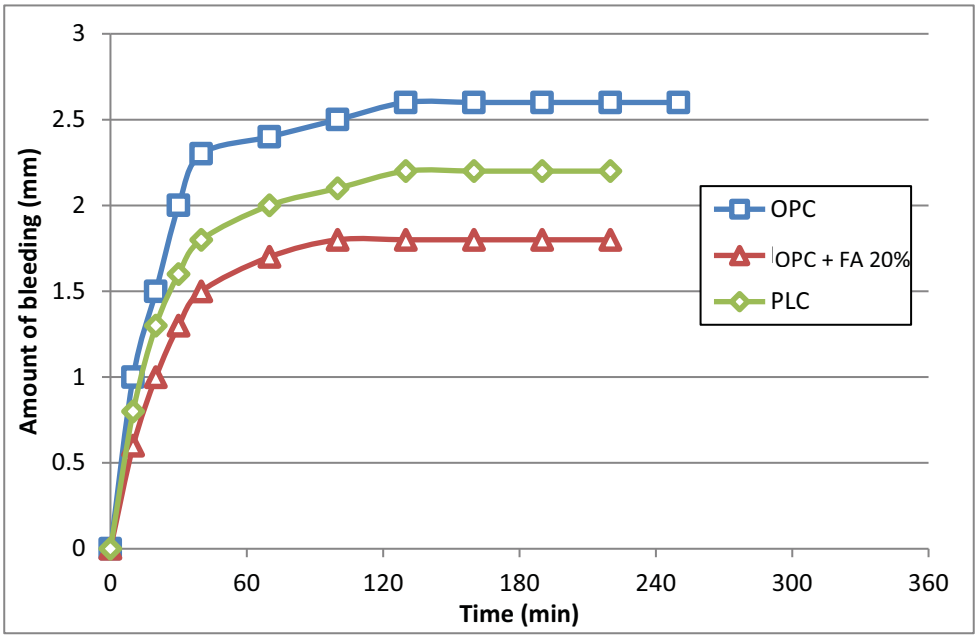


**Figure 5.1 Measured bleeding for OPC, PLC and OPC + FA 20%**

It was noted that the addition of fly ash has caused a reduction in bleeding. The amount of bleeding when PLC was used also lower compared to OPC. This matches with the experimental investigations carried out by other researches regarding the bleeding behavior for different cement types. (Lohitha & Joshi, 1997 and Hooton et al, 2007). In this chapter the plastic shrinkage behavior of OPC and fly ash blended cement concrete will be discussed.

Due to the addition of fly ash which is finer than cement particles, bleeding is reduced. The factor that accounts for the fineness in the bleeding model is the regression coefficient corresponding to sand/aggregate ratio (s/a). In the normal OPC mix, the s/a ratio was 40% and it was increased to 48% in the Fly ash blended mix to adjust for the decrease in amount of bleeding. Table 5.1 shows the regression coefficients and $K_o$ and $\beta$ factors calculated for two different mixes.

i) W/C = 50%
ii) Sand / Aggregate (by volume ) = 40% & 48%
iii) Unit water content = 205 kg
iv) Depth (H) = 100mm

**Table 5.1Parameters for the bleeding model for OPC and OPC + 20% FA**

| Factor | OPC | | OPC + 20% FA | |
|---|---|---|---|---|
| | $\lambda_{Ko}$ | $\lambda_{\beta}$ | $\lambda_{Ko}$ | $\lambda_{\beta}$ |
| Water / cement ratio (w/c) | 1.0 | 1.0 | 1.0 | 1.0 |
| Unit water content (W) | 8.4 | 0.6 | 8.4 | 0.6 |
| Sand/Aggregate ratio (s/a) | 1.7 | 0.75 | 0.77 | 1.09 |
| Depth (H) | 0.28 | 0.46 | 0.28 | 0.46 |
| $K_o$ (m/min) | $5.094 \times 10^{-5}$ | | $2.307 \times 10^{-5}$ | |
| $\beta$ (kgf/m$^2$) | $2.681 \times 10^{3}$ | | $3.896 \times 10^{3}$ | |

Modeled bleeding behavior is shown in Figure 5.2 and it matches with the experimental results. Although the bleeding model was modified to match with the reduction of bleeding due to fly ash, further investigations are needed to include a separate factor to account for the change in cement type for the bleeding model.

## 5.3 Strain development model for concrete with OPC and Fly ash blended cement

For modeling purposes an evaporation rate of 1.0 kg/m$^2$/hr was selected as it was mentioned as the threshold limit of evaporation where precautions are required against plastic shrinkage cracking. Combined evaporation and bleeding behavior for two different concrete mixes are shown in Figure 5.3 and 5.4.

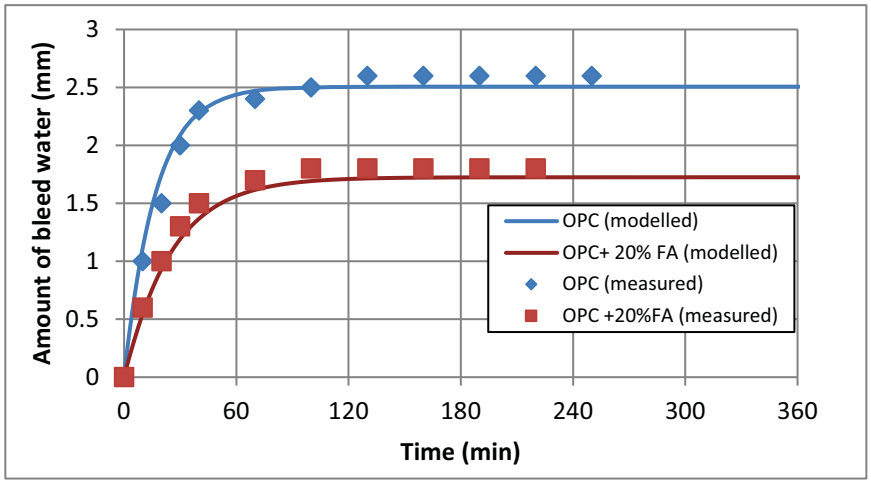


**Figure 5.2 Modelled bleeding behaviour for OPC and OPC + 20%FA**

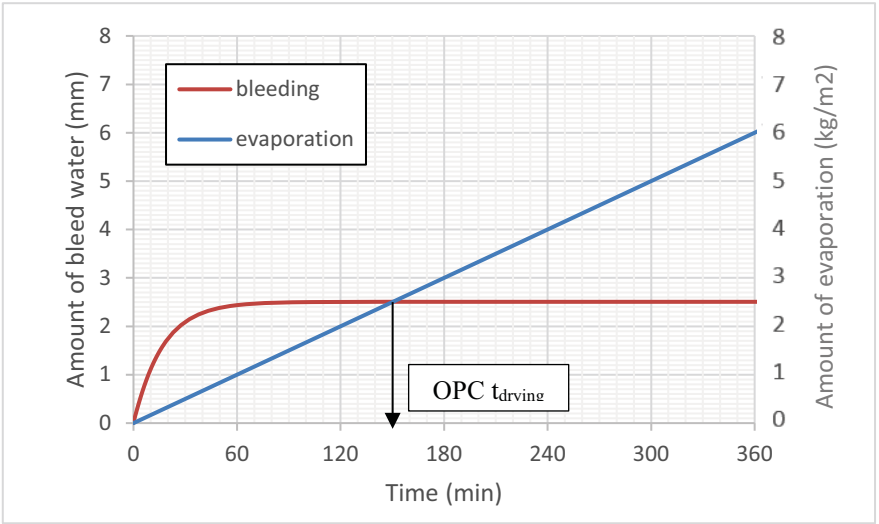


**Figure 5.3 Combined bleeding and evaporation for OPC**

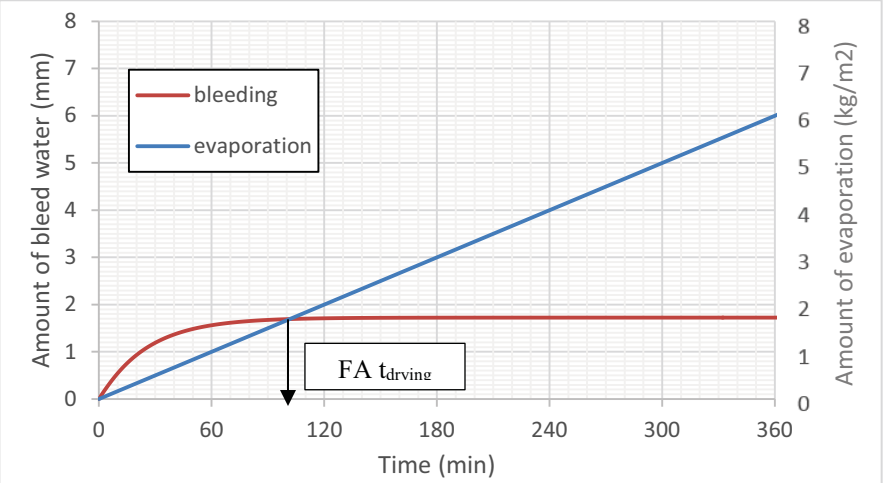


**Figure 5.4 Combined bleeding and evaporation for OPC+ 20% FA**

It can be seen from the Figures 5.3 & 5.4 that the starting point of drying for Fly ash blended concrete occurs earlier than OPC (for FA $t_{drying}$ = 100min and for OPC $t_{drying}$ = 150min). That is because, the bleeding was reduced in the fly ash blended mix and therefore for the same evaporation rate, the bleed water quickly gets evaporated in fly ash blended concrete relative to the OPC mix. After the point of drying, capillary pressure starts to develop and the rate of capillary pressure development was found as 0.41 kPa/min for the given evaporation rate using Figure 4.10 in chapter 04. For OPC, the lower and upper limits of capillary pressure (-10kPa and -45kPa) were reached at t= 175 min and t=260min respectively whereas for Fly ash blended mix the lower and upper limits of capillary pressure (-30kPa and -65kPa) were reached at t= 170 min and t=260min respectively (see Figures 5.5 and 5.6).

Capillary pressure development rate = 0.41 kPa/min

Time taken to achieve a capillary pressure of -10kPa ($t_{1,OPC}$) = 10/0.41 = 24.4 min

Time taken to achieve a capillary pressure of -45kPa ($t_{2,OPC}$) = 45/0.41 = 109.8 min

$T_{1,OPC}$ = OPC $t_{drying}$ + $t_{1,OPC}$ = 150 + 24.4 = 174.4 min ≈ 175 min

$T_{2,OPC}$ = OPC $t_{drying}$ + $t_{2,OPC}$ = 150 + 109.8 = 259.8 min ≈ 260 min

Time taken to achieve a capillary pressure of -30kPa ($t_{1,FA}$) = 30/0.41 = 72.2 min

Time taken to achieve a capillary pressure of -65kPa ($t_{2,FA}$) = 65/0.41 = 158.5 min

$T_{1,FA}$ = FA $t_{drying}$ + $t_{1,FA}$ = 100 + 72.2 = 172.2 min ≈ 170 min

$T_{2,FA}$ = FA $t_{drying}$ + $t_{2,FA}$ = 100 + 158.5 = 258.5 min ≈ 260 min

Volume of moisture evaporated for the above time intervals were calculated and shown in Table 5.2. A sample having a size of 1000mm x 1000mm x 100mm was used to model the shrinkage behavior. Volumetric contraction was modeled in finite element analysis software Abaqus as discussed in chapter 04 and the results are shown in Figures 5.7 & 5.8. Detailed calculations according to the method proposed in chapter 04 are given in Appendix C. Volumetric shrinkage obtained from the model was converted into equivalent horizontal shrinkage in the top layer of concrete and presented in Figures 5.9 and 5.10 along with the tensile strain capacity found from the experiment. Developed strain has two limits, i.e. upper bound and lower bound, as the capillary pressure development was assumed to terminate at its upper and lower limits as discussed in chapter 04. Therefore the actual strain developed in the specimen could lie between these two limits.

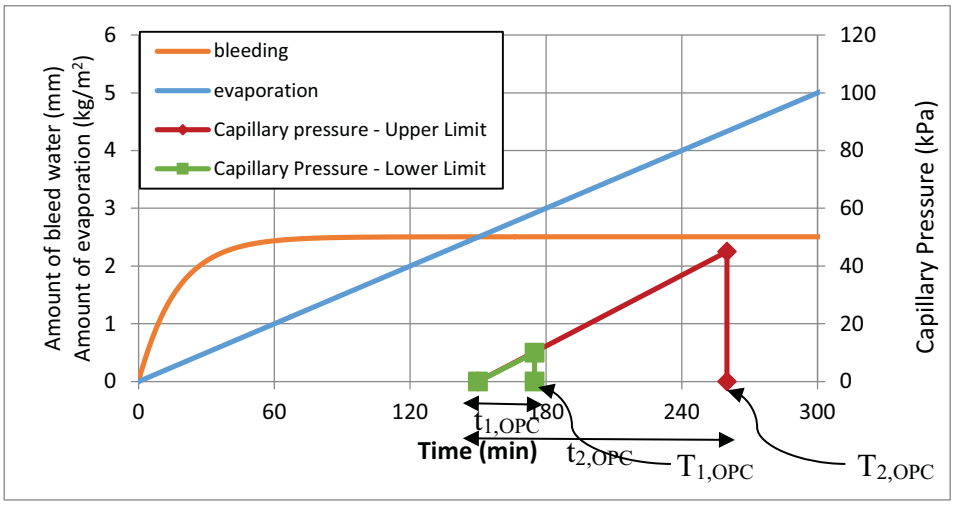


**Figure 5.5 Modelled bleeding and evaporation with capillary pressure limits for OPC**

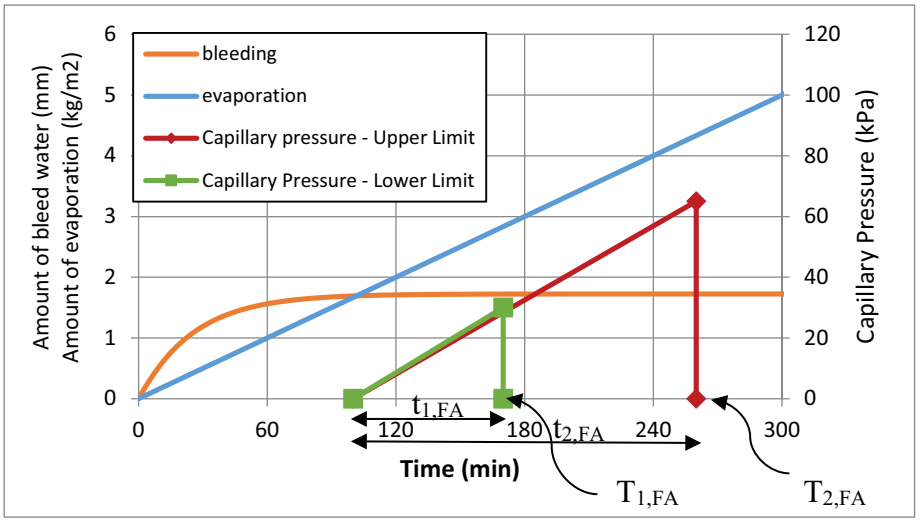


**Figure 5.6 Modelled bleeding and evaporation with capillary pressure limits for OPC+FA 20%**

**Table 5.2 Volumetric contraction for OPC and OPC + FA 20%**

| | OPC | | | OPC + 20% Fly Ash | | |
|---|---|---|---|---|---|---|
| | t = 150 min | t=175 min | t=260 min | t = 100 min | t=170 min | t=260 min |
| Total evaporation (kg/m2) | 2.5 | 2.92 | 4.33 | 1.7 | 2.83 | 4.33 |
| Total bleed volume (kg/m2) | 2.5 | 2.5 | 2.5 | 1.7 | 1.7 | 1.7 |
| Total contraction (kg/m2) | 0 | 0.42 | 1.83 | 0 | 1.13 | 2.63 |
| contraction for Δt (kg/m2) | 0 | 0.42 | 1.41 | 0 | 1.13 | 1.5 |
| Total contraction for Δt (mm3) | 0 | 420000 | 1410000 | 0 | 1130000 | 1500000 |

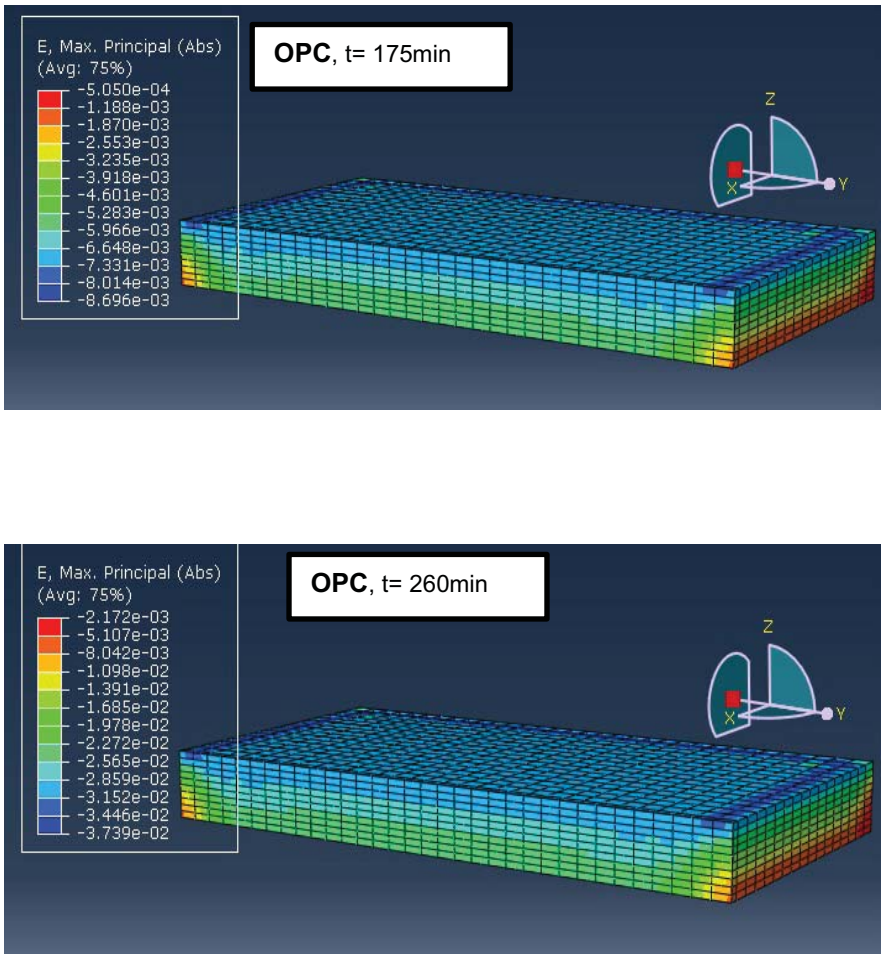


**Figure 5.7 Results of FE analysis for OPC**

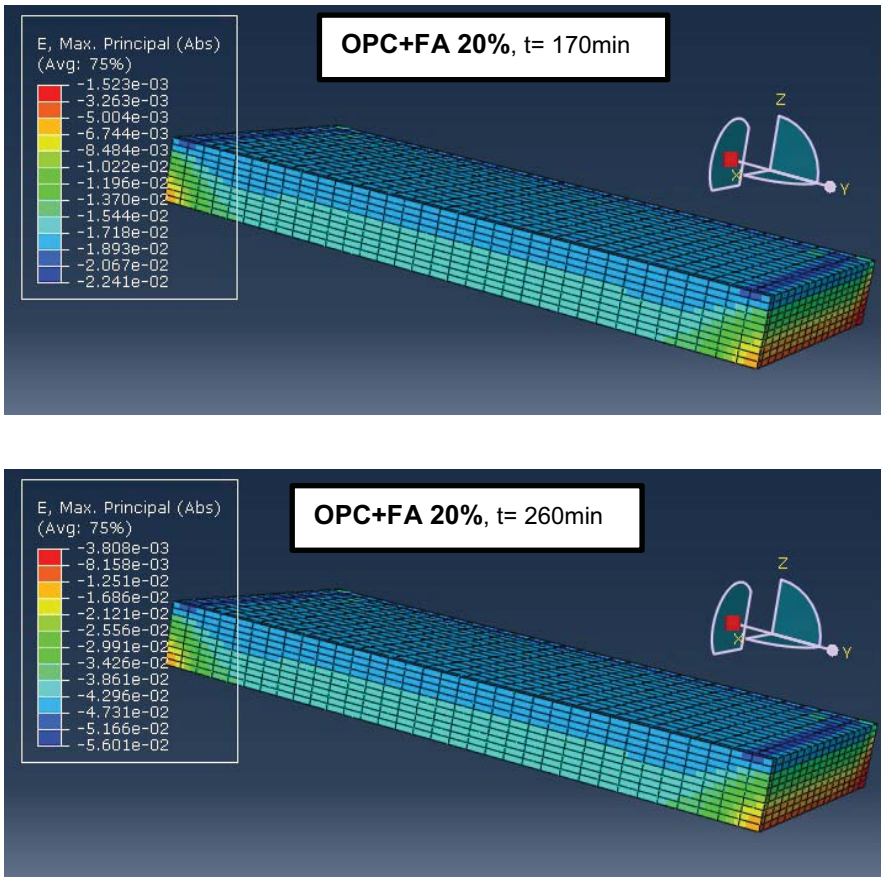


**Figure 5.8 Results of FE analysis for OPC + FA 20%**

## 5.4 Risk of plastic shrinkage cracking for concrete with OPC and OPC + 20% Fly ash

According the results, the tensile strain developed in OPC does not exceed the tensile strain capacity (Fig. 5.9); hence the risk of cracking is low. In concrete with fly ash the upper bound of the tensile strain developed almost reach the tensile strain capacity (Fig. 5.10). However, the results don't show that it definitely exceed the tensile strain capacity, hence the risk of cracking is not significantly high.

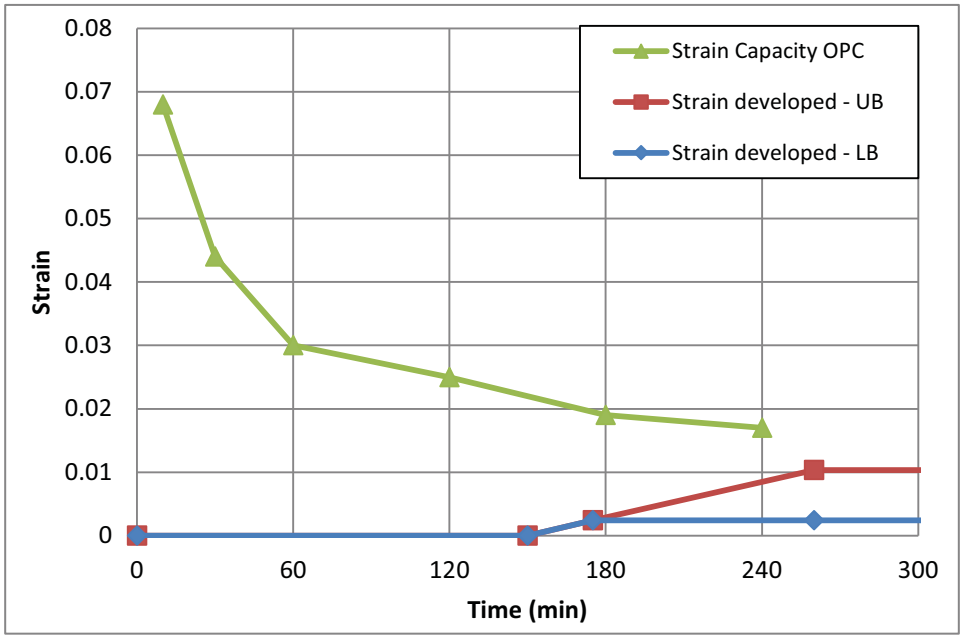


**Figure 5.9 Shrinkage strain and Tensile strain capacity for OPC**

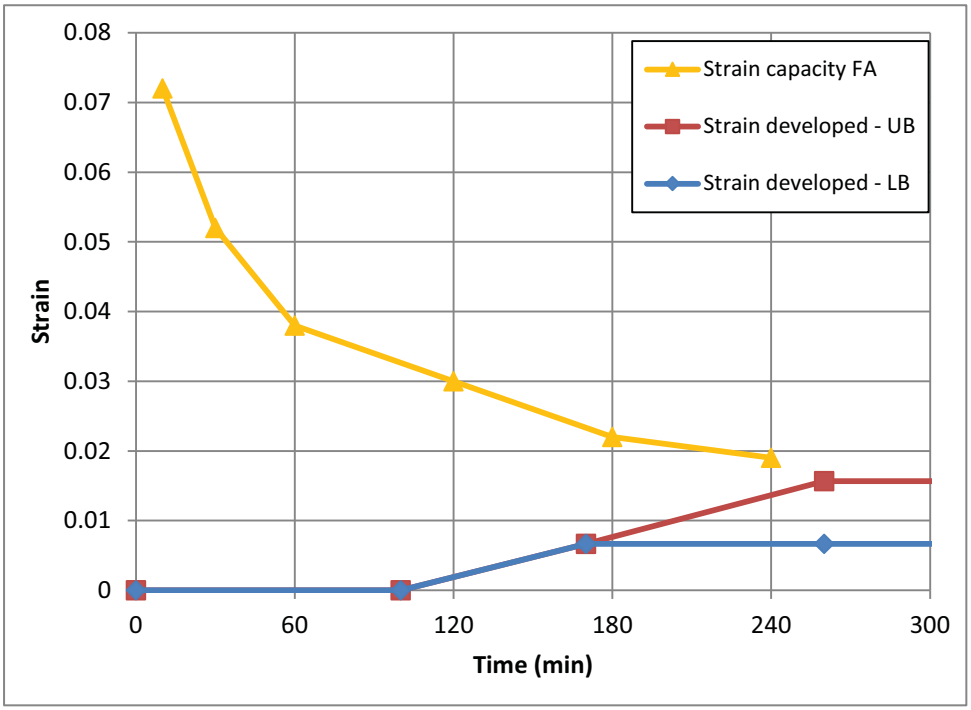


**Figure 5.10 Shrinkage strain and Tensile strain capacity for OPC + FA 20%**

In order to make a comparison between OPC and Fly ash blended concrete all the tensile strain capacities and developed tensile strain for both cases were expressed in one graph. (See Figure 5.11). According to Fig. 5.11, although there is an increase in

strain capacity in concrete with fly ash (maximum increase being 27% at 1 hour and 12% at 4 hours), the developed strain has increased by 63% at 4 hours. It can also be noted that the strain development in fly ash blended concrete starts earlier than that of OPC concrete.

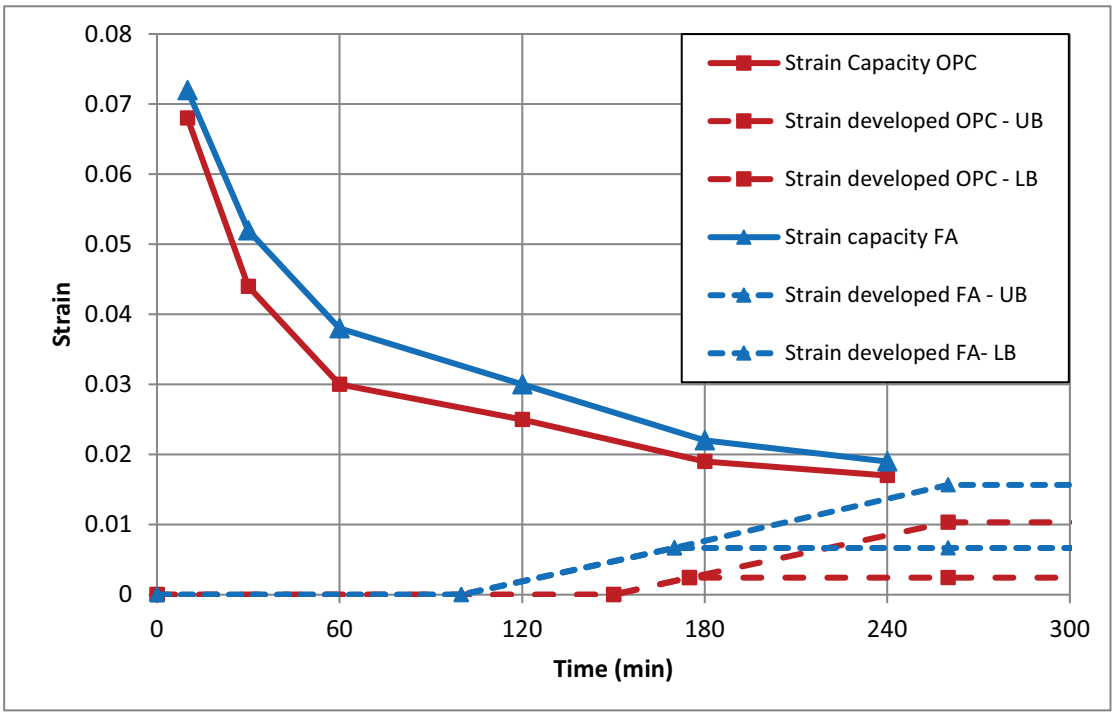


**Figure 5.11 Strain development and strain capacities for OPC and OPC + 20% Fly ash blended concrete**

### 5.4.1 Effect of depth of the concrete on plastic shrinkage cracking

Furthermore, to find out the effect of depth of the concrete to the plastic shrinkage cracking, the same concrete mix with OPC was considered and the depth was increased from 100mm to 200mm. Same procedure was adopted and detailed calculations are given in Appendix D. Variation of calculated bleeding combined with the same evaporation as before is shown in Figure 5.12.

It can be seen from the results that the amount of bleeding has been significantly increased with the increase of depth. That resulted a delay of the starting time of drying and it is well beyond 330 min whereas for 100mm thick sample it was 150 min.

Modeling of shrinkage development was not done as the shrinkage starts after about 5.5 hours and the strain capacities of fresh concrete were taken only up to 4 hours.

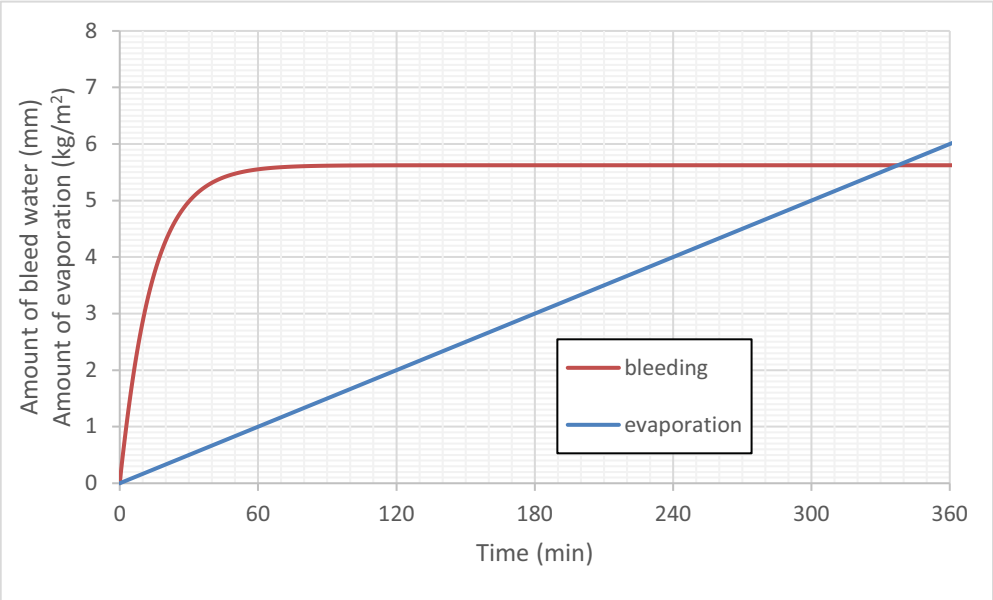


**Figure 5.12 Bleeding and evaporation for OPC: 200mm thickness**

## 5.5 Summary

Based on the experimental results on tensile strain capacity of fresh concrete and the model to simulate the shrinkage development in fresh concrete, an attempt was made to evaluate the risk of plastic shrinkage cracking in concrete made with OPC and fly ash blended cement. Although there was an increase in strain capacities in fly ash blended cement, there was a reduction in bleeding which resulted in an increase of developed tensile strain. Percentage increase of developed strain was greater than the percentage increase of strain capacity for concrete with fly ash when compared with concrete made with OPC. Developed strain almost reached the strain capacity in concrete with fly ash whereas for OPC, it was well below the strain capacity. Therefore it was concluded that the risk of plastic shrinkage cracking was high when fly ash was added. Furthermore, the model was used to find the effect of the depth of concrete on plastic shrinkage cracking. Results showed that when the depth was increased, the amount of bleeding increased and this resulted in further delaying the starting point of drying and as a result risk of plastic shrinkage cracking was reduced when the depth was increased.

# 6 CONCLUSIONS AND RECOMMENDATIONS

## 6.1 Conclusions

The plastic shrinkage mechanism of fresh concrete was studied and a method was proposed to evaluate the risk of plastic shrinkage cracking based on the tensile strain capacity of fresh concrete and tensile strain development of fresh concrete.

A test method was developed to measure tensile strain capacity of fresh concrete with improved accuracy as it measures the local strain at the location of cracking. Results showed that strain capacity decreases non-linearly with time as concrete transforms from semi-liquid state and plastic state. The influence of cement type, fine aggregate type and mortar phase of concrete for the strain capacity were investigated and the outcome revealed that when the fines in the cement mortar increases, the strain capacities also increase. This behaviour was observed when OPC was replaced by ultra-fine particles and river sand was replaced by finer manufactured sand. Addition of fines resulted in an increase of cohesiveness which was the reason for the increase in tensile strain capacity. OPC and PLC cement types showed more or less similar strain capacity while, in mortar phase, it was significantly higher at the early age and after 2 hours, concrete and mortar showed similar behaviour. The reason could be that, after mortar has reached the initial setting time, coarse aggregate has no effect on strain capacity. This proved the fact that mortar phase governed the plastic shrinkage behavior which was suggested by many other researchers.

Second phase of the study was to develop a model to simulate the tensile strain development in fresh concrete. Bleeding and evaporation which are the two factors governing the strain development were modeled and the subsequent moisture deficit was incorporated in a finite element model to predict the strain development. The model was verified by comparing the calculated strain values with experimentally measured strain from an independent research. In the model, an upper and lower limit for shrinkage was defined based on the capillary pressure development in fresh concrete and experimentally measured shrinkage was within these limits which further confirmed the accuracy of the model.

A case study was done to evaluate the risk of plastic shrinkage cracking of OPC and concrete with fly ash by modeling the strain development and comparing them with the strain capacities obtained from the test. Results indicate that although the strain capacity was increased when fly ash was added, the strain developed was also increased by a higher percentage which suggests that the risk of cracking is higher in concrete with fly ash.

Furthermore, another attempt was made to find the influence of concrete depth for the cracking risk and the model showed that with the increase of the depth of concrete, risk of plastic shrinkage cracking reduces. Similarly, the model can be incorporated to evaluate the risk of plastic shrinkage cracking for different mix proportions, different thicknesses of concrete exposed to different environmental conditions.

## 6.2 Further Studies

- Further studies are needed regarding modeling the capillary pressure development in fresh concrete and establishing an accurate relationship between evaporation and capillary pressure development rate. Furthermore the range of limits for maximum capillary pressure should be verified using experimental investigations.
- The plastic shrinkage cracking risk of PLC should be evaluated using the model since many cases have been reported on plastic shrinkage cracking in concrete elements where PLC was used.
- Accuracy of the model can be further improved by doing experiments and comparing the results with the predicted risk of cracking.

# REFERENCES


Almusallam, A.. et al., 1998. Effect of mix proportions on plastic shrinkage cracking of concrete in hot environments. *Construction and Building Materials*, 12(6–7), pp.353–358.

American Concrete Institute, 1999. *ACI manual of concrete practice.* Detroit : ACI.

Boshoff, W.P., 2012. Plastic Shrinkage Cracking of Concrete. , (December).

Byfors, J., 1980. Plain concrete at early stages*,* Sweden: *Swedish Cement and Concrete Research Institute*.

Combrinck, R. & Boshoff, W.P., 2013. Typical plastic shrinkage cracking behaviour of concrete. *Magazine of Concrete Research*, 65(8), pp.486–493.

Dias, W.P.S., 2003. Influence of mix and environment on plastic shrinkage cracking. *Magazine of Concrete Research*, 55(4), pp.385–394.

Dippenaar, D., 2015. The tensile properties of early age concrete and the experimental apparatus required for its determination. , (March).

Greim, M., 2011. Measuring the Early Shrinkage of Mortars. *Third International Drymix Mortar Conference*.

Hannat, D., Branch, J. & Mulheron, M., 1999. Equipment for testing of fresh concrete. *Magazine of Concrete Research,* Issue 51, pp. 263-267.

Hammer, T. A., 2007. Deformations, strain capacity and cracking of concrete in plastic and early hardening phases*,* s.l.: *Norwegian University of Science and Technology*

Hooton, R.D., Nokken, M. & Thomas, M. D. A., 2007**.** *Portland Limestone Cemenet : State of the art Report.* Toronto : Cement Association of Canada.

Huang, Y. et al., 2010. Optical strain gauge vs. traditional strain gauges for concrete elasticity modulus determination. *Optik - International journal for light and electron optics,* 121(18), pp. 1635-1641.

Holt, E. & Leivo, M., 2004. Cracking risks associated with early age shrinkage. *Cement and Concrete Composites*, 26(5), pp.521–530.

Josserand, L., Coussy, O. & de Larrard, F., 2006. Bleeding of concrete as an ageing consolidation process. *Cement and Concrete Research*, 36(9), pp.1603–1608.

Kasai, Y., Yokoyama, K. & Matsui, I., 1972. *Tensile Properties of early-age concrete.* Japan, International conference on mechanical behaviour of materials, The society of Materials Science.

Kwak, H.-G. & Ha, S.-J., 2006. Plastic shrinkage cracking in concrete slabs. Part I: a numerical model. *Magazine of Concrete Research*, 58(8), pp.505–516.

Kwak, H.-G. & Ha, S.-J., 2006. Plastic shrinkage cracking in concrete slabs. Part II: numerical experiment and prediction of occurance. *Magazine of Concrete Research*, 58(8), pp.517–532.

Lohitha, R.P., & Joshi R.C., 1997**.** *Fly Ash in Concrete: Production, Properties and Uses.*

Mehta, P. & Monteiro, P., 2013. Concrete: Microstructure, Properties, and Materials. 4th ed. s.l.:*McGrawHill education.*

Morris, P.H. & Dux, P.F., 2010. Analytical solutions for bleeding of concrete due to consolidation. *Cement and Concrete Research*, 40(10), pp.1531–1540.

Powers, T. C., 1968. *The Properties of Fresh Concrete.* New York: John Wiley & Sons. Inc.

Radocea, A., 1994. A model of plastic shrinkage. *Magazine of Concrete Research*, 46(167), pp.125–132.

Roziere, E., Cortas, R. & Loukili, A., 2015. Tensile behaviour of early age concrete: New methods of investigation. *Cement and Concrete Composites*, 55, pp.153–161.

Slowik, V., Schmidt, M. & Fritzsch, R., 2008. Capillary pressure in fresh cement-based materials and identification of the air entry value. *Cement and Concrete Composites*, 30(7), pp.557–565.

Tan, T. S., Wee, T. H., Tan, S. A., Tam C. T. & Lee, S. L. A., 1987. Consolidation model for bleeding of cement paste. *Advances in cement research*, 1(1), pp. 18-26.

Topçu, I.B. & Elgün, V.B., 2004. Influence of concrete properties on bleeding and evaporation. *Cement and Concrete Research*, 34(2), pp.275–281.

Uno, P.J., 1998. Plastic shrinkage cracking and evaporation formulas. *ACI Materials Journal*, 95(4), pp.365–375.

Wittmann, F.H., 1976. On the action of capillary pressure in fresh concrete. *Cement and Concrete Research*, 6(1), pp.49–56.

# APPENDIX A

## A.1 Summary of results for tensile strain capacities

| | Strain Capacity - Method 2 | | | | | | | | Strain Capacity - Method 1 | | |
|---|---|---|---|---|---|---|---|---|---|---|---|
| Time (min) | OPC | Mortar | MSand 20% | MSand 50% | FA 20% | FA 40% | FA 100% | PLC | OPC | PLC | FA 20% |
| 10 | 0.068 | 0.09 | 0.065 | 0.072 | 0.072 | 0.082 | 0.09 | 0.065 | 0.099 | 0.098 | 0.107 |
| 30 | 0.044 | 0.087 | 0.047 | 0.051 | 0.052 | 0.06 | 0.071 | 0.044 | 0.086 | 0.09 | 0.1 |
| 60 | 0.03 | 0.081 | 0.031 | 0.044 | 0.038 | 0.049 | 0.055 | 0.031 | 0.081 | 0.08 | 0.09 |
| 120 | 0.025 | 0.029 | 0.026 | 0.032 | 0.03 | 0.035 | 0.042 | 0.024 | 0.06 | 0.055 | 0.07 |
| 180 | 0.019 | 0.022 | 0.02 | 0.026 | 0.022 | 0.026 | 0.03 | 0.017 | 0.051 | 0.05 | 0.062 |
| 240 | 0.017 | 0.016 | 0.019 | 0.021 | 0.019 | 0.021 | 0.023 | 0.015 | 0.042 | 0.035 | 0.051 |

## A.2 Calculation of tensile strain capacities

| | OPC (Method 2) | | | | | | | | |
|---|---|---|---|---|---|---|---|---|---|
| | At start | | | | At failure | | | | Strain |
| | No. of pixels | Tape (cm) | Distance from center (cm) | Scale factor | No. of pixels | Tape (cm) | Distance from center (cm) | Scale factor | |
| **10 min** | 280 | 104 | -35.6 | 1.0598 | 295 | 107.5 | -39.55 | 1.0665 | 0.068 |
| | | 114 | | | | 118 | | | |
| **30 min** | 305 | 83.3 | -12.1 | 1.0203 | 317 | 84.8 | -13.95 | 1.0234 | 0.044 |
| | | 94.1 | | | | 96.1 | | | |
| **1 Hour** | 261 | 86 | -14.15 | 1.0238 | 268 | 86.7 | -15.1 | 1.0254 | 0.030 |
| | | 95.3 | | | | 96.3 | | | |
| **2 hour** | 267 | 103.5 | -34.35 | 1.0577 | 273 | 104.5 | -34.45 | 1.0579 | 0.025 |
| | | 113 | | | | 114.2 | | | |
| **3 Hour** | 247 | 105 | -35 | 1.0588 | 251 | 105.3 | -35.3 | 1.0593 | 0.019 |
| | | 113.8 | | | | 114.3 | | | |
| **4 Hour** | 261 | 103.3 | -33.45 | 1.0562 | 265 | 103.4 | -33.5 | 1.0563 | 0.017 |
| | | 112.6 | | | | 112.8 | | | |
| | **PLC (Method 2)** | | | | | | | | |
| **10 min** | 357 | 100.8 | -30.65 | 1.0515 | 376 | 103.3 | -33.9 | 1.057 | 0.065 |
| | | 113.7 | | | | 116.7 | | | |
| **30 min** | 344 | 100.4 | -28.7 | 1.0482 | 356 | 102.8 | -31.6 | 1.0531 | 0.044 |
| | | 113 | | | | 116 | | | |
| **1 Hour** | 347 | 87.6 | -19.3 | 1.0324 | 354 | 89.2 | -24.4 | 1.041 | 0.031 |
| | | 100 | | | | 102.2 | | | |
| **2 hour** | 310 | 100.8 | -31.9 | 1.0536 | 315 | 101.2 | -35.5 | 1.0597 | 0.024 |
| | | 112 | | | | 112.4 | | | |
| **3 Hour** | 291 | 102.7 | -30.95 | 1.052 | 295 | 103 | -32 | 1.0538 | 0.017 |
| | | 113.4 | | | | 115 | | | |
| **4 Hour** | 301 | 114.9 | -43.6 | 1.0733 | 305 | 115 | -43.6 | 1.0733 | 0.015 |
| | | 126.5 | | | | 126.6 | | | |
| | **FA 20% (Method 2)** | | | | | | | | |
| **10 min** | 308 | 101.8 | -31.15 | 1.0524 | 326 | 105 | -35.15 | 1.0591 | 0.072 |
| | | 113.5 | | | | 117.1 | | | |
| **30 min** | 299 | 102 | -32.05 | 1.0539 | 312 | 104.3 | -34.1 | 1.0573 | 0.052 |
| | | 113.1 | | | | 115.9 | | | |
| **1 Hour** | 274 | 103.5 | -32.4 | 1.0545 | 282 | 105.4 | -35.2 | 1.0592 | 0.038 |
| | | 113.7 | | | | 118 | | | |
| **2 hour** | 342 | 87.2 | -19.1 | 1.0321 | 349 | 89 | -23.45 | 1.0394 | 0.030 |
| | | 99 | | | | 101.9 | | | |
| | 380 | 76.4 | -5.8 | 1.0097 | 388 | 76.5 | -6 | 1.0101 | 0.022 |

| | | | | | | | | | |
|---|---|---|---|---|---|---|---|---|---|
| **3 Hour** | | 90 | | | | 90.5 | | | |
| **4 Hour** | 360 | 86.2 | -16.2 | 1.0272 | 366 | 86.8 | -16.75 | 1.0282 | 0.019 |
| | | 100 | | | | 100.7 | | | |

**FA 40% (Method 2)**

| | | | | | | | | | |
|---|---|---|---|---|---|---|---|---|---|
| **10 min** | 312 | 100.4 | -30.65 | 1.0515 | 333 | 103.6 | -34.8 | 1.0585 | 0.082 |
| | | 112.9 | | | | 117 | | | |
| **30 min** | 308 | 99.5 | -29.15 | 1.049 | 323 | 102.4 | -32.35 | 1.0544 | 0.060 |
| | | 111 | | | | 114.3 | | | |
| **1 Hour** | 337 | 80.2 | -10 | 1.0168 | 352 | 81.7 | -11.9 | 1.02 | 0.049 |
| | | 92.4 | | | | 94.5 | | | |
| **2 hour** | 291 | 102.7 | -30.95 | 1.052 | 299 | 103.6 | -33.3 | 1.056 | 0.035 |
| | | 113.4 | | | | 116 | | | |
| **3 Hour** | 311 | 101.5 | -29.75 | 1.05 | 318 | 102 | -30.25 | 1.0508 | 0.026 |
| | | 112.8 | | | | 113.5 | | | |
| **4 Hour** | 270 | 105.4 | -35.35 | 1.0594 | 275 | 105.9 | -35.45 | 1.0596 | 0.021 |
| | | 114.5 | | | | 115 | | | |

**FA 100% (Method 2)**

| | | | | | | | | | |
|---|---|---|---|---|---|---|---|---|---|
| **10 min** | 312 | 101 | -30.8 | 1.0518 | 334 | 105.2 | -37.1 | 1.0624 | 0.090 |
| | | 113.2 | | | | 119.4 | | | |
| **30 min** | 342 | 98.2 | -28.15 | 1.0473 | 363 | 100.5 | -30.05 | 1.0505 | 0.071 |
| | | 109.1 | | | | 111.6 | | | |
| **1 Hour** | 300 | 101.9 | -31.9 | 1.0536 | 314 | 104.2 | -33.45 | 1.0562 | 0.055 |
| | | 112.9 | | | | 115.7 | | | |
| **2 hour** | 337 | 82.2 | -11.55 | 1.0194 | 350 | 83 | -12.5 | 1.021 | 0.042 |
| | | 93.5 | | | | 94.4 | | | |
| **3 Hour** | 308 | 100.2 | -31.4 | 1.0528 | 314 | 101.2 | -35.8 | 1.0602 | 0.030 |
| | | 111.6 | | | | 112.6 | | | |
| **4 Hour** | 284 | 98.7 | -27.05 | 1.0455 | 288 | 99.1 | -31.4 | 1.0528 | 0.023 |
| | | 105.4 | | | | 105.9 | | | |

**Msand 20% (Method 2)**

| | | | | | | | | | |
|---|---|---|---|---|---|---|---|---|---|
| **10 min** | 296 | 90 | -21.75 | 1.0366 | 312 | 92.8 | -25.4 | 1.0427 | 0.065 |
| | | 100.5 | | | | 104 | | | |
| **30 min** | 314 | 90.7 | -20.75 | 1.0349 | 327 | 92.4 | -22.4 | 1.0376 | 0.047 |
| | | 102.2 | | | | 104.4 | | | |
| **1 Hour** | 317 | 80.2 | -8.05 | 1.0135 | 326 | 81.1 | -8.9 | 1.015 | 0.031 |
| | | 91.5 | | | | 92.7 | | | |
| **2 hour** | 293 | 104 | -36.55 | 1.0614 | 299 | 104.4 | -37.95 | 1.0638 | 0.026 |
| | | 114.1 | | | | 114.5 | | | |
| **3 Hour** | 307 | 102 | -31.05 | 1.0522 | 312 | 102.4 | -32.1 | 1.0539 | 0.020 |
| | | 113.3 | | | | 113.8 | | | |

| | | | | | | | | | |
|---|---|---|---|---|---|---|---|---|---|
| **4 Hour** | 346 | 99.3 | -29.65 | 1.0498 | 352 | 99.3 | -29.8 | 1.0501 | 0.019 |
| | | 112 | | | | 112.3 | | | |

**Msand 40% (Method 2)**

| | | | | | | | | | |
|---|---|---|---|---|---|---|---|---|---|
| **10 min** | 323 | 90.2 | -18.45 | 1.031 | 343 | 92.1 | -21.75 | 1.0366 | 0.072 |
| | | 101.9 | | | | 104.6 | | | |
| **30 min** | 343 | 100.8 | -31.95 | 1.0537 | 358 | 103.3 | -33.35 | 1.0561 | 0.051 |
| | | 113.5 | | | | 116.4 | | | |
| **1 Hour** | 313 | 101.6 | -32.3 | 1.0543 | 326 | 103.5 | -31.35 | 1.0527 | 0.044 |
| | | 113 | | | | 115.2 | | | |
| **2 hour** | 302 | 95.6 | -25.4 | 1.0427 | 309 | 98.5 | -27.9 | 1.0469 | 0.030 |
| | | 106.2 | | | | 109.3 | | | |
| **3 Hour** | 359 | 100.1 | -31.15 | 1.0524 | 367 | 100.4 | -32.05 | 1.0539 | 0.026 |
| | | 113.2 | | | | 113.7 | | | |
| **4 Hour** | 318 | 101.3 | -26.15 | 1.0439 | 324 | 101.4 | -26.6 | 1.0447 | 0.021 |
| | | 103 | | | | 103.2 | | | |

**Mortar (Method 2)**

| | | | | | | | | | |
|---|---|---|---|---|---|---|---|---|---|
| **10 min** | 245 | 102.6 | -31.55 | 1.053 | 263 | 104.5 | -35.95 | 1.0604 | 0.090 |
| | | 110.9 | | | . | 113.4 | | | |
| **30 min** | 238 | 105 | -34.1 | 1.0573 | 254 | 109.7 | -40.35 | 1.0678 | 0.087 |
| | | 113.6 | | | | 119 | | | |
| **1 Hour** | 256 | 88.1 | -19.75 | 1.0332 | 274 | 90.6 | -22.9 | 1.0385 | 0.081 |
| | | 97 | | | | 100.4 | | | |
| **2 hour** | 204 | 98 | -28.35 | 1.0476 | 209 | 98.7 | -29.35 | 1.0493 | 0.029 |
| | | 105.5 | | | | 106.4 | | | |
| **3 Hour** | 238 | 104.1 | -34.05 | 1.0572 | 242 | 104.3 | -35.8 | 1.0602 | 0.022 |
| | | 113 | | | | 113.3 | | | |
| **4 Hour** | 228 | 107 | -32.8 | 1.0551 | 231 | 107.3 | -33.6 | 1.0565 | 0.016 |
| | | 105.4 | | | | 105.7 | | | |

**OPC (Method 1)**

| | | | | | | | | | |
|---|---|---|---|---|---|---|---|---|---|
| **10 min** | 187 | 90.2 | -25.65 | 1.0431 | 202 | 95.3 | -31.9 | 1.0536 | 0.099 |
| | | 112.3 | | | | 117.5 | | | |
| **30 min** | 194 | 56.7 | 16.1 | 1.0271 | 210 | 57.4 | 15.4 | 1.0259 | 0.086 |
| | | 62.3 | | | | 63 | | | |
| **1 Hour** | 187 | 100.8 | -28.5 | 1.0479 | 200 | 102.9 | -30.75 | 1.0517 | 0.081 |
| | | 106.2 | | | | 108.6 | | | |
| **2 hour** | 196 | 101.3 | -29 | 1.0487 | 206 | 103.4 | -31.25 | 1.0525 | 0.060 |
| | | 106.7 | | | | 109.1 | | | |
| **3 Hour** | 199 | 88.8 | -19.05 | 1.032 | 208 | 90.2 | -20.5 | 1.0345 | 0.051 |
| | | 94.3 | | | | 95.8 | | | |
| **4 Hour** | 182 | 109.5 | -34.1 | 1.0573 | 188 | 111 | -36.8 | 1.0618 | 0.042 |
| | | 114.7 | | | | 116.6 | | | |

**PLC (Method 1)**

| | | | | | | | | | |
|---|---|---|---|---|---|---|---|---|---|
| **10 min** | 279 | 102 | -31.1 | 1.0523 | 301 | 106.2 | -36.6 | 1.0615 | 0.098 |
| | | 109.6 | | | | 114.6 | | | |
| **30 min** | 280 | 86.5 | -16.3 | 1.0274 | 302 | 89.2 | -20.1 | 1.0338 | 0.090 |
| | | 94.1 | | | | 97.2 | | | |
| **1 Hour** | 331 | 106.5 | -35.25 | 1.0592 | 352 | 110.2 | -39.8 | 1.0669 | 0.080 |
| | | 115.4 | | | | 119.8 | | | |
| **2 hour** | 269 | 52.4 | 23.65 | 1.0397 | 283 | 53.1 | 22.8 | 1.0383 | 0.055 |
| | | 59.5 | | | | 60.5 | | | |
| **3 Hour** | 253 | 88.9 | -14.8 | 1.0249 | 264 | 90.5 | -16.95 | 1.0285 | 0.050 |
| | | 95.7 | | | | 97.6 | | | |
| **4 Hour** | 262 | 101.6 | -27.95 | 1.047 | 270 | 103.2 | -29 | 1.0487 | 0.035 |
| | | 109.1 | | | | 110.8 | | | |

**FA 20% (Method 1)**

| | | | | | | | | | |
|---|---|---|---|---|---|---|---|---|---|
| **10 min** | 290 | 73.3 | -4.1 | 1.0069 | 319 | 75.9 | -6.85 | 1.0115 | 0.107 |
| | | 80.9 | | | | 83.8 | | | |
| **30 min** | 320 | 106.2 | -38 | 1.0639 | 346 | 110.2 | -42.3 | 1.0711 | 0.100 |
| | | 115 | | | | 119.6 | | | |
| **1 Hour** | 285 | 99.3 | -28.15 | 1.0473 | 306 | 103.3 | -32.95 | 1.0554 | 0.090 |
| | | 107 | | | | 111.8 | | | |
| **2 hour** | 187 | 103 | -29.1 | 1.0489 | 198 | 105.5 | -31.75 | 1.0534 | 0.070 |
| | | 108.2 | | | | 111 | | | |
| **3 Hour** | 212 | 101.1 | -29.8 | 1.0501 | 223 | 103.5 | -32.2 | 1.0541 | 0.062 |
| | | 107.1 | | | | 109.5 | | | |
| **4 Hour** | 214 | 106.7 | -34.05 | 1.0572 | 223 | 108.8 | -36.2 | 1.0608 | 0.051 |
| | | 112.8 | | | | 115 | | | |

# APPENDIX B – BLEEDING MODEL FOR THE EXPERIMENT BY SLOWIK (SLOWIK et al., 2008)

| INPUT DATA | |
|---|---|
| $K_o$ (m/min) | 1.68E-06 |
| β (kgf/m³) | 3.42E+03 |
| $e_o$ | 0.225 |
| $\gamma_w$ (kgf/m³) | 1000 |
| $\gamma_s$ (kgf/m³) | 3100 |
| Δt (min) | 2 |
| Δz (m) | 0.01 |

| Constants | | |
|---|---|---|
| $\Delta t/(\Delta z)^2$ | 2.00E+04 | Stability condition ; $\Delta t/(\Delta z)^2 < \gamma_w/(2\beta K_o)$ |
| $\gamma_w/(2\beta K_o)$ | 8.69E+04 | |
| $\beta K_o \Delta t/\gamma_w \Delta z^2$ | 0.11501516 | |
| | | |
| $(\gamma_w-\gamma_s)\Delta z/\beta$ | -6.14E-03 | |

| Height (m) | Time (min) | 0 | 2 | 4 | 6 | 8 | 10 | | 60 | 120 | 180 | 240 |
|---|---|---|---|---|---|---|---|---|---|---|---|---|
| | 0 | 0.225 | 0.225 | 0.225 | 0.225 | 0.225 | 0.225 | | 0.225 | 0.225 | 0.225 | 0.225 |
| | 0.01 | 0.225 | 0.225 | 0.225 | 0.225 | 0.225 | 0.224999 | | 0.223883 | 0.2222 | 0.221057 | 0.220304 |
| | 0.02 | 0.225 | 0.225 | 0.225 | 0.225 | 0.224991 | 0.224968 | | 0.222211 | 0.218998 | 0.216848 | 0.215433 |
| | 0.03 | 0.225 | 0.225 | 0.225 | 0.224919 | 0.224784 | 0.224615 | | 0.219446 | 0.215039 | 0.212141 | 0.210235 |
| | 0.04 | 0.225 | 0.225 | 0.224294 | 0.223668 | 0.223106 | 0.222592 | | 0.215129 | 0.21006 | 0.206763 | 0.204595 |
| | 0.05 | 0.225 | 0.218858 | 0.218151 | 0.217526 | 0.216964 | 0.21645 | | 0.208987 | 0.203918 | 0.20062 | 0.198453 |
| | | | | | | | | | | | | |
| | | 0.01225 | 0.01225 | 0.01225 | 0.01225 | 0.01225 | 0.01225 | | 0.012244 | 0.012236 | 0.01223 | 0.012227 |
| | | 0.01225 | 0.01225 | 0.01225 | 0.01225 | 0.01225 | 0.01225 | | 0.01223 | 0.012206 | 0.01219 | 0.012179 |
| | | 0.01225 | 0.01225 | 0.01225 | 0.01225 | 0.012249 | 0.012248 | | 0.012208 | 0.01217 | 0.012145 | 0.012128 |
| | | 0.01225 | 0.01225 | 0.012246 | 0.012243 | 0.012239 | 0.012236 | | 0.012173 | 0.012125 | 0.012095 | 0.012074 |
| | | 0.01225 | 0.012219 | 0.012212 | 0.012206 | 0.0122 | 0.012195 | | 0.012121 | 0.01207 | 0.012037 | 0.012015 |
| | | | | | | | | | | | | |
| | Σ(1 + e(z,t))Δz | 61.25 | 61.21929 | 61.20869 | 61.1985 | 61.18862 | 61.17899 | | 60.97663 | 60.80756 | 60.69619 | 60.62294 |
| | s(t) (mm) | h0 - Σ(1 + e(z,t))Δz | 0 | 0.030711 | 0.041307 | 0.051498 | 0.061375 | 0.071007 | | 0.27337 | 0.442443 | 0.553815 | 0.627063 |

| | Time (min) | 300 | 360 | 420 | 480 | 540 | 600 | 660 | 720 |
|---|---|---|---|---|---|---|---|---|---|
| Height (m) | 0 | 0.225 | 0.225 | 0.225 | 0.225 | 0.225 | 0.225 | 0.225 | 0.225 |
| | 0.01 | 0.219809 | 0.219483 | 0.219269 | 0.219128 | 0.219036 | 0.218975 | 0.218935 | 0.218908 |
| | 0.02 | 0.214503 | 0.213891 | 0.213489 | 0.213224 | 0.21305 | 0.212936 | 0.21286 | 0.212811 |
| | 0.03 | 0.208981 | 0.208157 | 0.207615 | 0.207258 | 0.207024 | 0.20687 | 0.206768 | 0.206702 |
| | 0.04 | 0.20317 | 0.202232 | 0.201616 | 0.20121 | 0.200944 | 0.200768 | 0.200653 | 0.200577 |
| | 0.05 | 0.197027 | 0.19609 | 0.195474 | 0.195068 | 0.194801 | 0.194626 | 0.194511 | 0.194435 |
| | | | | | | | | | |
| | $(1 + e(z,t))\Delta z$ | 0.012224 | 0.012222 | 0.012221 | 0.012221 | 0.01222 | 0.01222 | 0.01222 | 0.01222 |
| | | 0.012172 | 0.012167 | 0.012164 | 0.012162 | 0.01216 | 0.01216 | 0.012159 | 0.012159 |
| | | 0.012117 | 0.01211 | 0.012106 | 0.012102 | 0.0121 | 0.012099 | 0.012098 | 0.012098 |
| | | 0.012061 | 0.012052 | 0.012046 | 0.012042 | 0.01204 | 0.012038 | 0.012037 | 0.012036 |
| | | 0.012001 | 0.011992 | 0.011985 | 0.011981 | 0.011979 | 0.011977 | 0.011976 | 0.011975 |
| | | | | | | | | | |
| | $\Sigma(1 + e(z,t))\Delta z$ | 60.57477 | 60.54309 | 60.52225 | 60.50855 | 60.49954 | 60.49361 | 60.48972 | 60.48715 |
| | | | | | | | | | |
| s(t) (mm) | $ho - \Sigma(1 + e(z,t))\Delta z$ | 0.675234 | 0.706913 | 0.727747 | 0.741449 | 0.750459 | 0.756385 | 0.760282 | 0.762845 |

# APPENDIX C – ANALYTICAL MODELS TO PREDICT VOLUMETRIC CONTRACTION FOR OPC AND OPC+20% FA

## OPC (1m x 1m x 100mm) – Volumetric Contraction from 150min to 175min

| Layers across the depth (cm) | top | *e* at t= 150 min | % of water | porosity | volume of water (mm3) | Volume loss (mm3) ; up to 175min | Temp. difference ($^0$C) | Thermal coefficient of expansion (α) |
|---|---|---|---|---|---|---|---|---|
| | 1 | 0.255 | 11.5626 | 0.2032 | 2031872.510 | 48562.80 | 10.00 | 4.856E-04 |
| | 2 | 0.2471683 | 11.2075 | 0.1982 | 1981836.066 | 47071.31 | 10.00 | 4.707E-04 |
| | 3 | 0.2393366 | 10.8523 | 0.1931 | 1931166.890 | 45579.82 | 10.00 | 4.558E-04 |
| | 4 | 0.2315047 | 10.4972 | 0.1880 | 1879852.571 | 44088.31 | 10.00 | 4.409E-04 |
| | 5 | 0.2236727 | 10.1421 | 0.1828 | 1827880.400 | 42596.76 | 10.00 | 4.260E-04 |
| | 6 | 0.2158406 | 9.7869 | 0.1775 | 1775237.376 | 41105.18 | 10.00 | 4.111E-04 |
| | 7 | 0.2080082 | 9.4318 | 0.1722 | 1721910.213 | 39613.56 | 10.00 | 3.961E-04 |
| | 8 | 0.2001755 | 9.0766 | 0.1668 | 1667885.335 | 38121.90 | 10.00 | 3.812E-04 |
| | 9 | 0.1923426 | 8.7215 | 0.1613 | 1613148.882 | 36630.18 | 10.00 | 3.663E-04 |
| | 10 | 0.1923426 | 8.7215 | 0.1613 | 1613148.882 | 36630.18 | 10.00 | 3.663E-04 |
| | bottom | | | | | Σ = 420000 | | |

## OPC (1m x 1m x 100mm) – Volumetric Contraction from 175min to 260min

| Layers across the depth (cm) | top | *e* at t= 175 min | % of water | porosity | volume of water (mm3) | Volume loss (mm3) ; up to 260min | Temp. difference ($^0$C) | Thermal coefficient of expansion (α) |
|---|---|---|---|---|---|---|---|---|
| | 1 | 0.247398 | 11.5449 | 0.1983 | 1983309.711 | 162782.99 | 33.52 | 4.856E-04 |
| | 2 | 0.239889 | 11.1945 | 0.1935 | 1934764.751 | 157842.78 | 33.53 | 4.707E-04 |
| | 3 | 0.232375 | 10.8439 | 0.1886 | 1885587.071 | 152898.45 | 33.55 | 4.558E-04 |
| | 4 | 0.224854 | 10.4929 | 0.1836 | 1835764.266 | 147950.00 | 33.56 | 4.409E-04 |
| | 5 | 0.217327 | 10.1417 | 0.1785 | 1785283.638 | 142997.44 | 33.57 | 4.260E-04 |
| | 6 | 0.209794 | 9.7901 | 0.1734 | 1734132.193 | 138040.76 | 33.58 | 4.111E-04 |
| | 7 | 0.202255 | 9.4383 | 0.1682 | 1682296.651 | 133079.99 | 33.59 | 3.96E-04 |
| | 8 | 0.194709 | 9.0862 | 0.1630 | 1629763.44 | 128115.13 | 33.61 | 3.81E-04 |
| | 9 | 0.187158 | 8.7338 | 0.1577 | 1576518.702 | 123146.23 | 33.62 | 3.66E-04 |
| | 10 | 0.187158 | 8.7338 | 0.1577 | 1576518.702 | 123146.23 | 33.62 | 3.66E-04 |
| | bottom | | | | | Σ = 1410000 | | |

## OPC +FA 20% (1m x 1m x 100mm) – Volumetric Contraction from 100min to 170min

| Layers across the depth (cm) | top | *e* at t= 100 min | % of water | porosity | volume of water (mm3) | Volume loss (mm3) ; up to 170min | Temp. difference ($^0$C) | Thermal coefficient of expansion (α) |
|---|---|---|---|---|---|---|---|---|
| | 1 | 0.255 | 11.0052 | 0.2032 | 2031872.510 | 124358.40 | 10.00 | 1.244E-03 |
| | 2 | 0.2497411 | 10.7782 | 0.1998 | 1998342.869 | 121793.76 | 10.00 | 1.218E-03 |
| | 3 | 0.2444765 | 10.5510 | 0.1964 | 1964492.809 | 119226.31 | 10.00 | 1.192E-03 |
| | 4 | 0.2392007 | 10.3233 | 0.1930 | 1930282.046 | 116653.39 | 10.00 | 1.167E-03 |
| | 5 | 0.2339086 | 10.0949 | 0.1896 | 1895672.209 | 114072.56 | 10.00 | 1.141E-03 |
| | 6 | 0.2285961 | 9.8656 | 0.1861 | 1860628.368 | 111481.74 | 10.00 | 1.115E-03 |
| | 7 | 0.2232596 | 9.6353 | 0.1825 | 1825120.446 | 108879.25 | 10.00 | 1.089E-03 |
| | 8 | 0.2178969 | 9.4039 | 0.1789 | 1789124.434 | 106263.97 | 10.00 | 1.063E-03 |
| | 9 | 0.2125068 | 9.1713 | 0.1753 | 1752623.359 | 103635.30 | 10.00 | 1.036E-03 |
| | 10 | 0.2125068 | 9.1713 | 0.1753 | 1752623.359 | 103635.30 | 10.00 | 1.036E-03 |
| | bottom | | | | | Σ = 1130000 | | |

## OPC +FA 20% (1m x 1m x 100mm) – Volumetric Contraction from 170min to 260min

| Layers across the depth(cm) | top | *e* at t= 170 min | % of water | porosity | volume of water (mm3) | Volume loss (mm3) ; up to 260min | Temp. difference ($^0$C) | Thermal coefficient of expansion (α) |
|---|---|---|---|---|---|---|---|---|
| | 1 | 0.235714 | 10.9749 | 0.1908 | 1907514.105 | 164623.52 | 13.24 | 1.244E-03 |
| | 2 | 0.231004 | 10.7556 | 0.1877 | 1876549.112 | 161333.84 | 13.25 | 1.218E-03 |
| | 3 | 0.226282 | 10.5357 | 0.1845 | 1845266.497 | 158035.78 | 13.26 | 1.192E-03 |
| | 4 | 0.221542 | 10.3151 | 0.1814 | 1813628.653 | 154725.90 | 13.26 | 1.167E-03 |
| | 5 | 0.216782 | 10.0934 | 0.1782 | 1781599.644 | 151401.06 | 13.27 | 1.141E-03 |
| | 6 | 0.211996 | 9.8706 | 0.1749 | 1749146.632 | 148058.53 | 13.28 | 1.115E-03 |
| | 7 | 0.207181 | 9.6464 | 0.1716 | 1716241.194 | 144696.15 | 13.29 | 1.09E-03 |
| | 8 | 0.202336 | 9.4208 | 0.1683 | 1682860.463 | 141312.38 | 13.30 | 1.06E-03 |
| | 9 | 0.19746 | 9.1938 | 0.1649 | 1648988.055 | 137906.42 | 13.31 | 1.04E-03 |
| | 10 | 0.19746 | 9.1938 | 0.1649 | 1648988.055 | 137906.42 | 13.31 | 1.04E-03 |
| | bottom | | | | | Σ = 1500000 | | |

# APPENDIX D – BLEEDING MODEL OPC – 200mm DEPTH

| INPUT DATA | |
|---|---|
| $K_0$ (m/min) | 1.38E-04 |
| β (kgf/m²) | 4.78E+03 |
| $e_0$ | 0.255 |
| $Y_w$ (kgf/m³) | 1000 |
| $Y_s$ (kgf/m³) | 3100 |
| Δt (min) | 0.25 |
| Δz (m) | 0.02 |

| Constants | | |
|---|---|---|
| $\Delta t/(\Delta z)^2$ | 6.25E+02 | Stability condition ; $\Delta t/(\Delta z)^2 < Y_w/(2\beta K_0)$ |
| $Y_w/(2\beta K_0)$ | 7.57E+02 | |
| $\beta K_0 \Delta t/Y_w \Delta z^2$ | 0.41308481 | |
| | | |
| $(Y_w-Y_s)\Delta z/\beta$ | -8.79E-03 | |

| Height (m) | Time (min) | 0 | 0.25 | 0.5 | 0.75 | 1 | 30 | 60 | 90 | 120 | 150 | 180 |
|---|---|---|---|---|---|---|---|---|---|---|---|---|
| | 0.02 | 0.255 | 0.255 | 0.255 | 0.255 | 0.255 | 0.255 | 0.255 | 0.255 | 0.255 | 0.255 | 0.255 |
| | 0.04 | 0.255 | 0.255 | 0.255 | 0.255 | 0.255 | 0.24748 | 0.246354 | 0.246228 | 0.246213 | 0.246212 | 0.246212 |
| | 0.06 | 0.255 | 0.255 | 0.255 | 0.255 | 0.255 | 0.239905 | 0.237702 | 0.237454 | 0.237427 | 0.237423 | 0.237423 |
| | 0.08 | 0.255 | 0.255 | 0.255 | 0.255 | 0.255 | 0.232221 | 0.229038 | 0.22868 | 0.22864 | 0.228635 | 0.228635 |
| | 0.10 | 0.255 | 0.255 | 0.255 | 0.255 | 0.255 | 0.22438 | 0.220356 | 0.219903 | 0.219853 | 0.219847 | 0.219846 |
| | 0.12 | 0.255 | 0.255 | 0.255 | 0.255 | 0.254381 | 0.216341 | 0.211651 | 0.211124 | 0.211065 | 0.211059 | 0.211058 |
| | 0.14 | 0.255 | 0.255 | 0.255 | 0.2535 | 0.252359 | 0.208072 | 0.202921 | 0.202343 | 0.202278 | 0.20227 | 0.202269 |
| | 0.16 | 0.255 | 0.255 | 0.25137 | 0.249239 | 0.247369 | 0.199548 | 0.194162 | 0.193557 | 0.193489 | 0.193482 | 0.193481 |
| | 0.18 | 0.255 | 0.246212 | 0.242581 | 0.24045 | 0.23858 | 0.19076 | 0.185374 | 0.184769 | 0.184701 | 0.184693 | 0.184693 |
| | | | | | | | | | | | | |
| $(1+e(z,t))\Delta z$ | | 0.0251 | 0.0251 | 0.0251 | 0.0251 | 0.0251 | 0.025025 | 0.025014 | 0.025012 | 0.025012 | 0.025012 | 0.025012 |
| | | 0.0251 | 0.0251 | 0.0251 | 0.0251 | 0.0251 | 0.024874 | 0.024841 | 0.024837 | 0.024836 | 0.024836 | 0.024836 |
| | | 0.0251 | 0.0251 | 0.0251 | 0.0251 | 0.0251 | 0.024721 | 0.024667 | 0.024661 | 0.024661 | 0.024661 | 0.024661 |
| | | 0.0251 | 0.0251 | 0.0251 | 0.0251 | 0.0251 | 0.024566 | 0.024494 | 0.024486 | 0.024485 | 0.024485 | 0.024485 |
| | | 0.0251 | 0.0251 | 0.0251 | 0.0251 | 0.025094 | 0.024407 | 0.02432 | 0.02431 | 0.024309 | 0.024309 | 0.024309 |
| | | 0.0251 | 0.0251 | 0.0251 | 0.025085 | 0.025067 | 0.024244 | 0.024146 | 0.024135 | 0.024133 | 0.024133 | 0.024133 |
| | | 0.0251 | 0.0251 | 0.025064 | 0.025027 | 0.024997 | 0.024076 | 0.023971 | 0.023959 | 0.023958 | 0.023958 | 0.023958 |
| | | 0.0251 | 0.025012 | 0.02494 | 0.024897 | 0.024859 | 0.023903 | 0.023795 | 0.023783 | 0.023782 | 0.023782 | 0.023782 |
| | | | | | | | | | | | | |
| | $\Sigma[1+e(z,t)]\Delta z$ | 200.8 | 200.7121 | 200.6032 | 200.5093 | 200.418 | 195.8165 | 195.2474 | 195.1835 | 195.1763 | 195.1755 | 195.1754 |
| s(t) (mm) | $h_0 - \Sigma[1+e(z,t)]\Delta z$ | 0 | 0.087884 | 0.196796 | 0.29071 | 0.382018 | 4.983458 | 5.552583 | 5.616517 | 5.623699 | 5.624506 | 5.624596 |